Numerical investigations of a swirling two-phase air-water upward flow in straight and convergent vertical pipe.

MANIMARAN, R., KUMAR, M.S., KARUNAMURTHY, K. and HOSSAIN, M.

2023

Numerical Investigations of a Swirling Two-Phase Air-Water Upward Flow in Straight and Convergent Vertical Pipe

R. Manimaran[1], M. Senthil Kumar[2], K. Karunamurthy[1], Mamdud Hossain[3]

[1]Thermal, Automotive and Energy Group, School of Mechanical Engineering, Vellore Institute of Technology, Chennai, India

[2]Materials and Manufacturing Group, School of Mechanical Engineering, Vellore Institute of Technology, Chennai, India

[3]Energy Research Group, School of Engineering, Robert Gordon University, Scotland, UK

Correspondence : Telephone/Fax : +91-44-39931555 E-Mail : manimaran.r@vit.ac.in

Abstract

In this study, a numerical study is presented to analyse the flow parameters such as longitudinal and transverse velocities, hydrodynamic pressure and volume fraction inside a vertical pipe. A vertical ascending swirl flow is established with the specified boundary conditions and compared between straight and convergent geometry pipes. Normalized film thickness is found to vary between 0.4 and 0.6, where the numerical output data from the present study resembles with wire-mesh sensor data from literature. Convergent pipe flow includes the variation of hydrodynamic pressure thereby affecting the slug and bubble flow region. Longitudinal and transverse velocities are plotted against time and compared at the three inspection planes near the inlet, mid-portion and outlet respectively. In order to understand the effectiveness of rotational effect of gas and liquid phases, the vorticity components are studied. Parameters such as Q-criterion and vortex stretching term indicate the straining and shearing flow near the peripheral and core regions. The temporal volume fraction variation at the output section indicates the increase in the output liquid yield of convergent pipe outlet by 17 %.

Keywords : gas-liquid two phase; swirl flow; volume fraction; straight circular pipe; convergent pipe; computational fluid dynamics

Introduction

Oil and gas flow into the bore-well when it is drilled into a reservoir in the oil extraction site. Thereafter oil refinery employs long pipes to extract oil to the earth's surface. Different phases of fluids exist in the pipe flows whereas oil production is significantly impacted by flow regime. For instance, the slug flow creates a significant pressure decrease in the surface system, and could even cause the well to shut down. Therefore, it is crucial to evaluate the pipe's two-phase upward flow. From the literature of two-phase fluid flows in pipe, different kinds of flow regime exist such as bubble flow, slug flow, churn flow and annular flows. Many literature have been dedicated to these flow regimes by experimental and numerical approaches. A brief look-up on the above mentioned flow regimes is discussed next.

The study is focused towards the liquid wetting of walls with the study of liquid fraction in pipe-cross section and impact of bubble forces. Adaze et al. (2019) observed the shear stress fluctuation with high amplitude in the vicinity of the pipe wall where the liquid phase dominates and gradually decreases towards the pipe centre before predicting the onset of film reversal to enable necessary actions to be taken to mitigate the problem of liquid loading. By positioning a gamma ray source and detector around the pipe, Adineh et al. (2015) detected

all transmitted and scattered gamma rays in all directions for all three modelled flow regimes. In order to give an adequate correction coefficient for the void measurement with higher precision for validation with experimental results, they also performed numerical modelling using the Monte-Carlo N-Particle algorithm. The frictional pressure drop can be predicted analytically using only the pipe's design, the physical characteristics of fluids, and their flow rates, according to Ameri and Tirandaz (2017) proposal. Recent experimental data and model predictions are compared, and the results demonstrate good agreement and significant improvement over the ideal core annular flow model. For Reynolds numbers in the range of 50,000 to 500,000, Atmani et al. (2022) proposed to extend the log-law modelling using local and unsteady values of the wall shear stress obtained from a stochastic model. This would improve the fluctuations and spatial distribution of turbulent structures inside the pipe. Cailly et al. (2020) performed a non-invasive imaging in an opaque pipe having two-phase flow that involves a small bubble flow imaging through opaque pipes. Two materials of very different acoustical properties were tested where the consistent target reconstruction is obtained for a specific pipe material. Many experimental studies on the investigation of two phase flow in a vertical pipe have been analysed next to arrive at significant physical phenomena, theoretical correlations and model developments.

To study the gas-liquid-hydrate flow issue in a vertical pipe, Cao et al. (2022) developed an integrated multiphase flow model that takes into account the coalescence and breakup of bubbles and hydrate particles. Results showed that during the flow process, the phase distribution grew uneven, and bubbles tended to collect in the middle of the pipe. For two-component two-phase slug flows in vertical pipes, Carlos et al. (2021) investigated the dynamics of a kerosene-water mixture in a vertical pipe flow. They used direct numerical simulations that were initialised with a slightly perturbed core-annular flow to produce mild turbulence and large-scale three-dimensional recirculation patterns. Dong and Hibiki (2018) discovered a strong correlation based on the traditional Reynolds and Chilton-Colburn analogies of heat transfer coefficient. Within a 30% error bound, the correlation accurately predicts 95.1% of the two-phase heat transfer data that have been gathered for flow regimes such bubbly, churn, and annular flow regimes. Dziubinski et al. (2004) presented a map for the determination of flow pattern for two-phase flow of gas and non-Newtonian liquid in the vertical pipe. Eidt et al. (2021) performed the wire-mesh experimental study and compared and validated a numerical model using a compressive discretization approach to capture the liquid-gas interface along with the Shear Stress Transport turbulence model to examine the dynamics of a liquid film flow. The stability and behaviour of the vertically rising liquid layer flow are influenced by the surface velocities of the liquid and gas. Gamma-ray studies utilising polyethylene phantoms were used by Faghihi et al. (2015) to study the two-phase flow within a vertical pipe in the homogeneous, stratified, and annular flow regimes to propose the novel correlations. Issa and Lucas (2009) conducted experiments over a wide range of water and air surface velocities for two pipe diameters (50 mm and 200 mm) and successfully built a one-dimensional test-solver to represent a two phase upward bubbly flow. For the coalescence and breakup processes, the new model gave more trustworthy values of the turbulence parameters. In a vertical circular pipe, Long et al. (2022) investigated the two-phase flow instabilities using a validated numerical scheme and experimental data. In the flow boiling system, transient responses of local circumstances were discussed. With the aid of wire-mesh sensor technology, Lucas et al. (2010) created a comprehensive database for steady-state upward air-water flows in a vertical pipe with an inner diameter of 195.3 mm using 48 different air and water mixtures with superficial velocities ranging from 0.0025 m/s to 3.2 m/s for air and 0.04 m/s to 1.6 m/s for water. This is the best benchmark to use when validating a poly-dispersed flow. Using ultrafast electron beam X-ray computed tomography,

Martin et al. (2020) reported an experimental analysis of adiabatic bubbly two-phase flow formation in a pipe with a ring-shaped and a baffle-shaped constriction at various surface velocities of gas and liquid. They used an advanced data processing technique to quickly extract gas holdup information from the two-phase flow image stack. In a study by Ohnuki and Akimoto (2000), the transitional properties of the flow pattern and phase distribution in upward air-water two-phase flow along a large vertical pipe were evaluated experimentally. However, no big bubbles are seen in the region with length to diameter ratio lower than 20, which corresponds to the developing region of the axial differential pressure curves. This is despite the flow conditions at which coalescence occurs being nearly identical to those found in small-scale pipes.

As the flow phenomena involves multiple components, the study of different flow characteristics is essential and several studies have explained the slug flow, annular flow and churn flow regimes in their work. In order to determine flow properties including slug length, slug frequency, void percent in liquid slugs, and Taylor bubble velocity, Rajab et al. (2018) derived the void fraction time series from wire mesh sensor and an electrical capacitance tomography sensors. The variation from the established slug flow models, particularly those created to forecast the gas holdup in liquid slugs, is caused by changes in the physical characteristics of the liquid phase. By solving the Cahn-Hilliard-Navier-Stokes equations, According to Pouryoussefi and Yuwen (2015), the fuzzy logic code accurately predicts the flow pattern by employing image processing techniques, and the renormalization group k-epsilon turbulence model yields the best results for turbulence modelling. In order to evaluate bubble size during the lateral migration of bubbles of various sizes beginning from the injection at the wall, Prasser et al. (2007) changed the surface velocities in a range covering flow regimes from bubbly to churn-turbulent flow. By contrasting cold air-water trials with steam-water testing at 65 bar, the influence of the fluid's physical characteristics was investigated. In a pipe with sudden expansion (40 mm to 90 mm), Rinne and Loth (1996) presented experimental data for vertical air-water bubbly flow obtained by fiber-optic sensors and calculated the local void fraction, local bubble velocity, local bubble frequency, bubble chord length, bubble size, and local interfacial area concentration. With the variously specified bubble shapes in the determination techniques, flows with void fractions exceeding 0.04 look plausible. Saidj et al. (2018) measured the average void fractions at nine axial positions on a 6 m long, 34 mm diameter pipe test section using conductance probes. By extracting the characteristics of the slug flow, the theoretical model of Brauner and Ullmann is found to be useful for predicting the slug flow regime. Using hot-film anemometry, Shawkat et al. (2007) investigated the liquid turbulence structure of air-water bubbly flow in a 200 mm diameter vertical pipe. Beginning with low wave numbers, the suppression gradually moves up to higher wave numbers as it is amplified. Sibel et al. (2021) assessed the capabilities of Eulerian-Eulerian computational fluid dynamics (CFD) two-phase flow simulation with the homogeneous Multiple Size Group Model and consideration of breakup and coalescence under three-dimensional flow conditions. However, the simulation results generally agree well upstream the obstacle, but downstream of the obstacle void fraction is over-predicted while bubble velocity is under-predicted and hence a further model improvement is needed. Wire mesh sensors were used by Szalinsk et al. (2010) to analyse air/water and air/silicone oil two-phase flow in a vertical pipe with a diameter of 67 mm and a length of 6 m. Time series and bubble size distribution data are used to determine the flow patterns for each of the flow rates. Hot-film anemometry was used by Tas-Koehler et al. (2021) to measure the velocity of liquids while ultrafast X-ray computed tomography was used to get information on the gas phase.

Several empirical studies are compared with the numerical counter-part cases to develop an innovative, robust and fast model. The computationally less expensive renormalization group k-epsilon model, which is suggested for the simulation of complicated flow scenarios, is found to perform similarly to the shear stress transport Reynolds stress model after comparing the experimental findings with the numerical investigation. Zeguai et al. (2020) used an experimental setup in a 1500 mm long capillary tube with a 3 mm inner diameter and various orientations with regard to gravity to study the evolution of two-phase flow patterns. Numerous two-phase flow patterns, including bubbly flow, slug flow, unstable annular flow, and annular flow, are shown and explained with the construction of two-phase flow maps.

In many reported studies, analyses have been performed on vertically rising pipe with diameters ranging from 3 mm to 200 mm and length to diameter ranging from 80 to 500. The flow regimes involved from bubble flow, slug flow, and churn flow to fully blown annular thin film flows in the vertical pipe. As the oil industry concentrates on the yield of crude oil, the output capacity from the tubing/pipe must be significant. Hence from a mechanical engineering point of view, the nature of pipe selection plays a crucial role with important parameters such as pipe diameter, pipe length, pipe material, pipe surface roughness and pipe section etc. The novelty of the study lies in the maximum extraction of liquid fraction component during the oil exploration. The hypothesis is verified in using an upward convergent pipe to arrive at the cumulative volume fraction at the output. Study of flow in constant area pipe/ducts is enormous and the flow in the convergent pipe is very limited. As already understood from the basic fluid mechanics, the convergent pipe can be selected to give higher velocity for a constant mass flow rate. Hence the present study focusses on the yield of liquid phase in a convergent vertical pipe using numerical approach. Towards the validation, the numerical study is initially checked with the published experimental results from literature. The main essence of this study is to understand the comparison of flow establishment between straight pipe and convergent pipe on flow velocity, hydrostatic pressure, volume fraction, vorticity, Q-criterion and vortex stretching using turbulent flow modelling approach.

Methodology

The geometrical configuration of the pipe is shown in Fig. 1, where the dimensions of circular and convergent pipes are identical at inlet but different at outlet. Planes A, B and C are shown in Fig. 1, where the averaged or sampling points of field variables such as velocity, volume fraction and pressure are compared. These planes are situated near inlet (5 mm away, plane A), middle of pipe (190 mm from inlet, plane B) and outlet (290 mm from inlet, plane C) respectively. Especially plane B is chosen at this location (190 mm from inlet) as per the literature (Eidt et al., 2021) where the results from wire-mesh experimental study are compared and validated in this study. Mesh independent studies are performed under coarse, intermediate and fine mesh categories as shown in Fig. 2. The parameter of choice for evaluation was the average liquid film thickness at the cross section 190 mm high from the bottom of the cyclonic chamber (Eidt et al., 2021). To make it easier to compare the data, the liquid film's average thickness was normalised using the cyclonic chamber radius (δ/R). Table 1 lists the δ/r values from the present openFOAM software results in the range close to the experimental outcome of Eidt et al. (2021). The fine mesh category involving the 1.8 million hexahedrons and 0.22 million quadrangles could meet the requirement on experimental results by Eidt et al. (2021) as the range of δ/r varies from 0.39-0.83 for j_l = 1.0 m/s, j_g = 0.5 m/s and 0.49-0.81 for j_l = 2.0 m/s, j_g = 0.5 m/s.

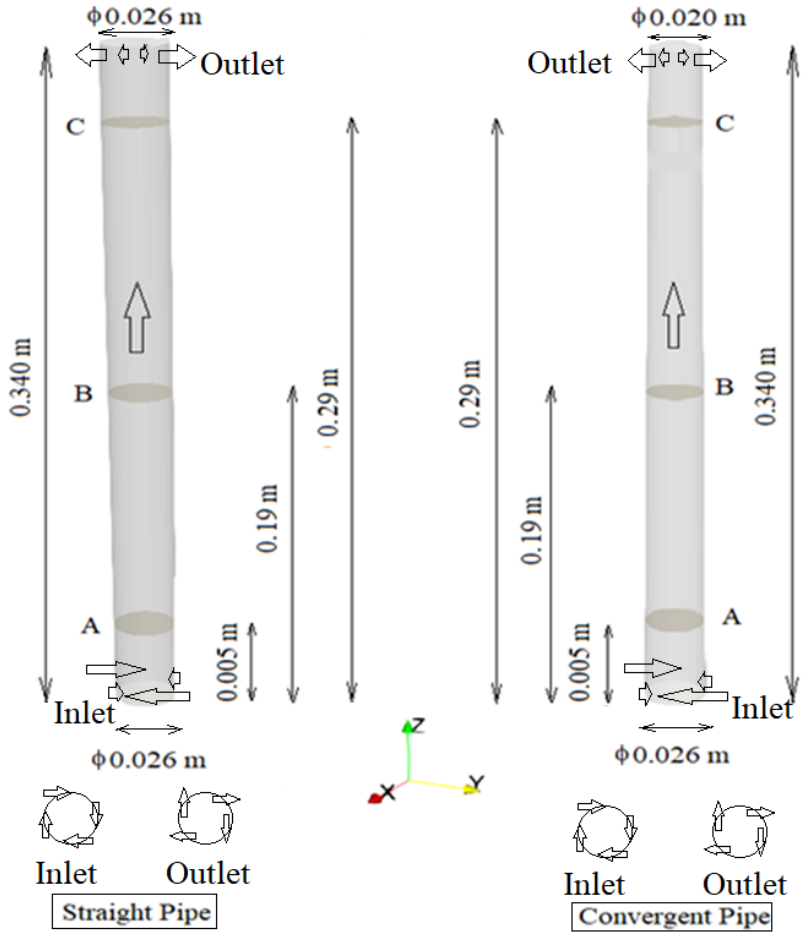

Fig. 1. Geometrical Configuration of Straight and Convergent pipes

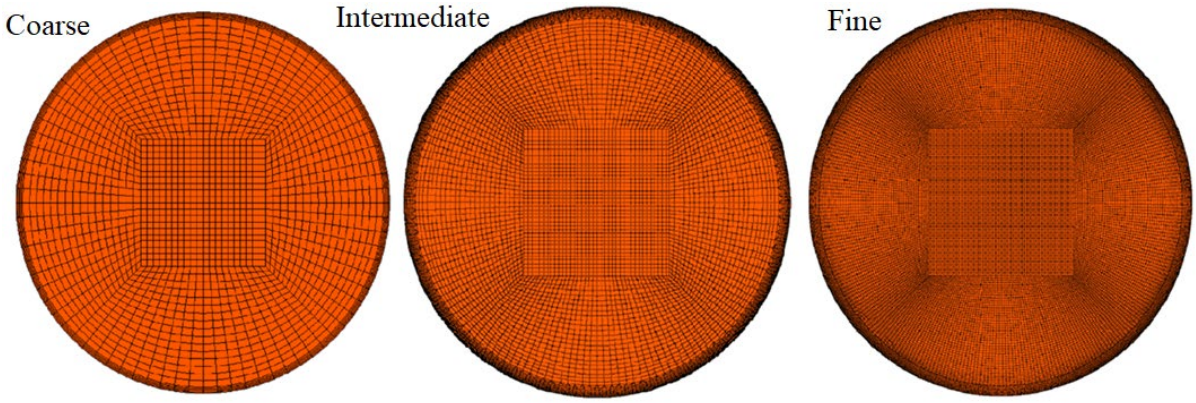

Fig. 2. Types of meshes employed in the study (shown in cross-section of pipe)

Table 1. Mesh independency tests

Mesh type	**Hexahedrons**	**Quadrangles**	**δ/r** (j_l = 1.0 m/s, j_g = 0.5 m/s)	**δ/r** (j_l = 2.0 m/s, J_g = 0.5 m/s)
Coarse	924800	146880	0.44-0.62	0.55-0.69
Intermediate	1223080	195240	0.42-0.68	0.54-0.74
Fine	1854060	224080	0.39-0.83	0.49-0.81

The present study involves the use of open-source software, OpenFOAM for the computation in the conservation of mass and momentum using finite volume method. For the two-phase flow approach, transient, three-dimensional and isothermal flow with volume of fluid modelling is adopted. Time step of 0.01 ms is carried out with the Courant number set to maximum limit of 0.2 for stability. This numerical study is aimed at predicting the flow regime i.e. bubble flow, slug flow and hence surface tension effect (σ = 0.07 N/m) is only considered during simulations. Towards the turbulence modelling, k-ω shear stress transport is used to calculate the vorticity and vortex stretching during the flow establishment. The CPU duration involves 30 hours for a flow simulation period of 1000 ms in Intel core i7-8700 at 3.20 GHz with 32 GB RAM under 64 bit MS Windows operating system. InterFOAM solver takes care of the two phase scenario i.e air and water with the following conservation equations.

$$\nabla \cdot u = 0 \quad (1)$$

The velocities in the fluid flow motion are found from the momentum equation below

$$D(\rho u)/Dt = -\nabla p + \nabla.\tau + \rho g + f_\sigma \quad (2)$$

Where u represents the velocity of phase, g the gravitational acceleration, p the pressure and τ the viscous and turbulent stresses. f_σ is the surface tension.

At the interface between gas and liquid, the density ρ is defined as follows:

$$\rho = \alpha\rho_1 + (1-\alpha)\rho_2 \quad (3)$$

where α denotes the volume fraction. Additional equation for volume fraction (α) is solved at every time step to arrive at the interface regions.

$$D\alpha/Dt = 0 \quad (4)$$

k-omega SST turbulence model is used to model the turbulence effects in the flow. The original k-ω SST turbulence model successfully predicts the bubble and slug flow due to well-balanced dissipation and diffusion effects around the free surface.

The turbulence specific dissipation rate (ω) equation is given by:

$$D(\rho\omega)/Dt = \nabla\cdot(\rho D_\omega \nabla\omega) + \rho\gamma G/\nu - 2/3\rho\gamma\omega(\nabla\cdot\underline{u}) - \rho\beta\omega^2 - \rho(F_1-1)CD_{k\omega} + S_\omega, \quad (5)$$

and the turbulence kinetic energy (k) by:

$$D(\rho k)/Dt = \nabla\cdot(\rho D_k \nabla k) + \rho G - 2/3\rho k(\nabla\cdot\underline{u}) - \rho\beta_*\omega k + S_k \quad (6)$$

The turbulence viscosity (v_t) is obtained using equation (7) as below.

$$\nu_t = a_1 k/\max(a_1\omega, b_1 F_{23} S) \quad (7)$$

The blending factors F_1 and F_{23} are used in the estimation of k and ω, while S refers to source term. For isotropic turbulence, the turbulence kinetic energy can be estimated by:

$$k=3/2(i/u_{ref})^2 \quad (8)$$

where I is the turbulence intensity, and u_{ref} a reference velocity. The turbulence specific dissipation rate, ω follows as:

$$\omega=k^{0.5}/C_\mu^{0.25}l \quad (9)$$

where C_μ is a constant equal to 0.09, and l a reference length scale.

Inlet is maintained with a superficial air flow velocity of 0.5 m/s and water flow velocity of 1 m/s, 2 m/s respectively. The same values are chosen in the mesh independency tests (Table 1) and validation test (Fig. 3). The inlet is maintained such that the swirling flow is established in both the straight and convergent pipes. The liquid and gas phases are specified at appropriate inlets at the bottom of the straight and convergent pipe cases. Similarly, the pressure outlet is maintained at atmospheric state at the top of the peripheral surface of the pipes, which may contain the liquid as well as the gaseous phases after a flow time period of 1 s. Three planes are selected for analyses at 0.005 m, 0.19 m and 0.29 m respectively from the bottom of the pipe.

Validation

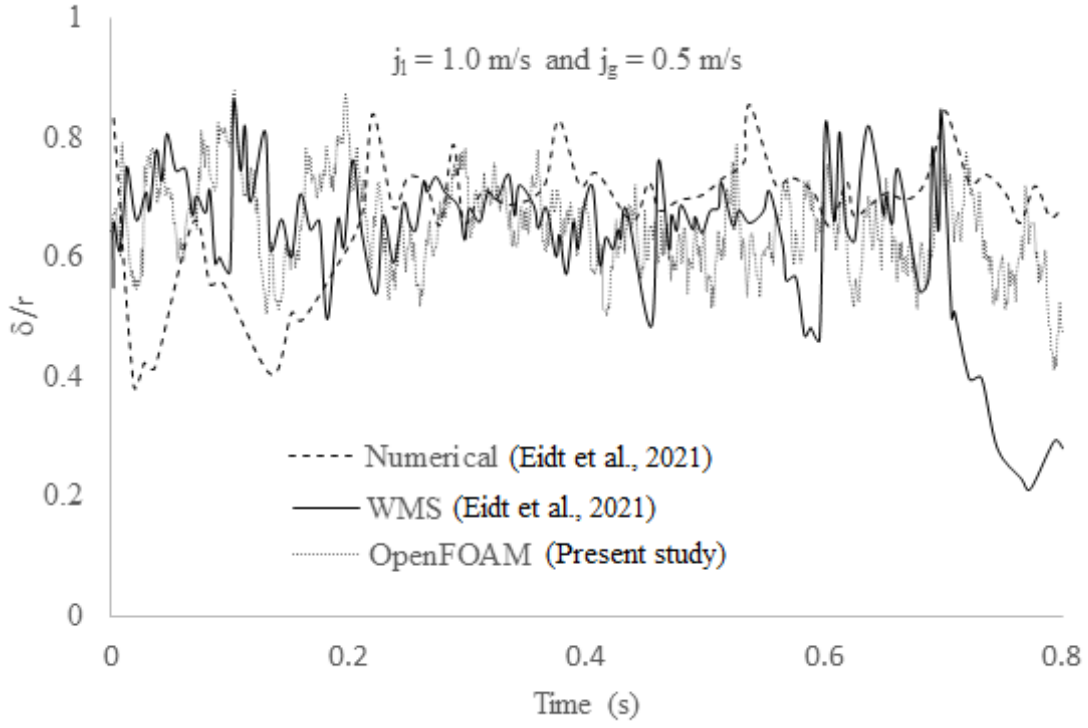

Fig. 3 Validation of bubble-slug transition flow from present study with literature

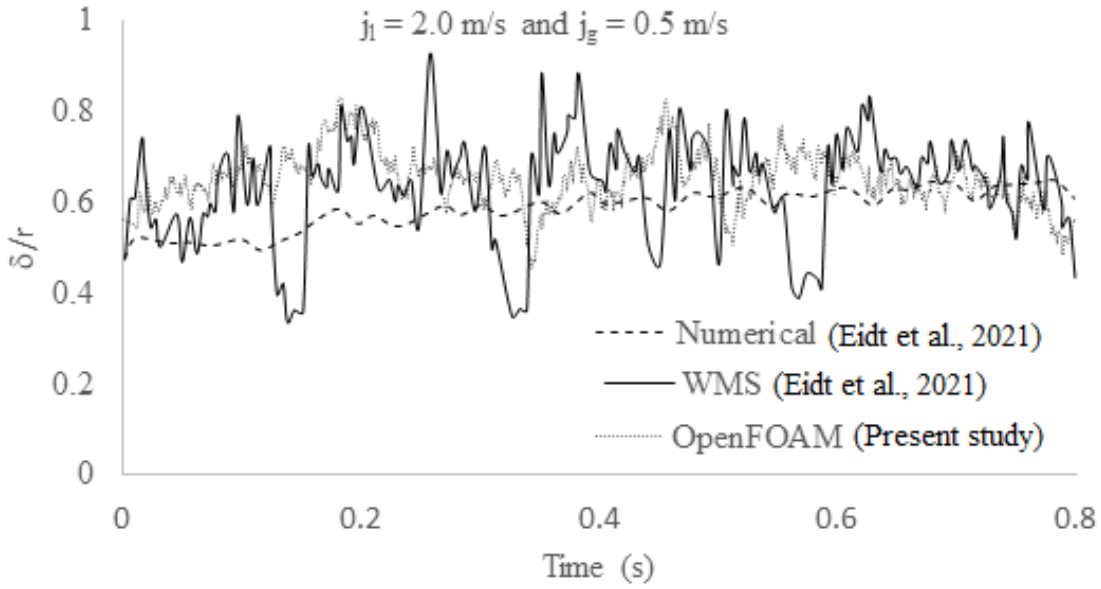

Fig. 4 Validation of bubbly flow from OpenFOAM study with literature

In this section, the numerical validation with the experimental data to bring reliability to the numerical results will be shown first. The validation test starts with the numerical simulation of bubble-slug transition flow using OpenFOAM. Test was performed with inlet superficial velocity of water at 1 m/s and air at 0.5 m/s. In Fig. 3, the dotted line represents the numerical simulation by Eidt et al. (2021), whereas the solid line indicates the experimental measurement of normalized film thickness (δ/r) by Eidt et al. (2021). The present study results are also plotted as thin closely spaced dotted line in Fig. 3. The time series data of the literature and present study goes hand in hand and does not deviate to the extent with the difference between the numerical and experimental data of the Eidt et al. (2021). Most of the data present in the series were within the experimental measurement coverage.

In the bubbly flow regime (Fig. 4), liquid superficial velocity is maintained at 2 m/s and the 0.5 m/s gas velocity is specified at the inlet. The non-dimensional film thickness is observed to be within the numerical and experimental datasets of Eidt et al. (2021). The present study trend in the seasonal variation also matches with the literature data trend. The wire-mesh sensor (WMS) data is found to vary between 0.4 and 0.6 in liquid film thickness ratio, while the present study trend is within the closer range to the WMS data.

Results and Discussion

The numerical results of the behavior of the swirling flow inside the cyclonic chamber and the liquid film formation will be analyzed. Finally, the variation of 3-components of vorticities, q-criterion and vortex stretching term will be evaluated as a function of the liquid and the gas superficial velocities. The objective of the study is to compare the liquid and gaseous phase flow features in the straight and convergent circular ducts. Upward flow inside the pipe against the gravitational force is maintained with water and gas inlets to simulate the situation of underground oil exploration. The ascending flow of water and gas is compared between the straight circular and convergent conical pipes. The angle of convergence is limited to 1.01^{o} for a length of 0.34 m pipe. Fig. 5 illustrates the sectional view of two-phase flow in straight and convergent pipes. In both cases, the gas is present at bottom core flow,

while the liquid film tends to form at the inner side of the top and bottom portions of the pipe. As the outlet pressure is maintained at 101325 Pa, the pressure distribution is uniform as shown in Fig. 6. The pressure decreases in the upward direction on the way towards the outlet.

A two phase friction multiplier or a two phase friction factor (homogeneous flow model) can be used to calculate the two phase frictional pressure decrease (separate flow model). In the gas-liquid swirling flow, there is a distinct interface between the gas and liquid phases, hence a different flow model is employed here. The variation in hydrodynamic pressure is shown in Fig. 7 as the slug and bubble flow region are found to be apparent in the top portion of the pipe. Hydrodynamic pressure is found as p-(ρgh), thus yielding to the dynamics of the flow condition. Longitudinal velocity appears to be higher at the core in both the straight and convergent cases due to the no-slip wall condition near the walls. The velocity (Fig. 8) appears to be moderately higher at the mid and top portions of the pipe for convergent pipe as compared to straight pipe. The interfacial drag force in the tangential direction between the gas and liquid phase is disregarded since the angular velocities of the gas and liquid phases are equal. As a result, the dominating reason for swirl decay in gas-liquid two-phase flow is the tangential friction force between the liquid film and the wall. The fluctuation of the flow patterns in the gas-liquid two-phase decaying swirl flow is strongly influenced by swirl decay. The flow velocities have a big impact on the formation of the swirling flow in the streamwise direction because they are directly related to the swirl decay. The differences in the distribution of gas and liquid line up with the rising fluid superficial velocities. Transverse velocity components in x and y directions (Fig. 9 and Fig. 10) are also higher in convergent as compared to straight pipe. The flow tends to accelerate in the convergent pipe as compared to straight pipe as per the conservation of mass of both phases, air and water. The velocity variation in the bottom, middle and top portions are analysed to understand the nature of flow from slug to bubble or annular. These variations are plotted in Fig. 11 for transverse-X velocity, Fig. 12 for transverse-Y velocity and Fig, 13 for longitudinal velocities. Intriguingly, the results produced by the computations using the various codes are remarkably comparable, and the gas velocity profiles are still predicted fairly well. Other than the turbulent viscosity, which is significantly altered in the middle region of the pipe as a result of the enhanced bubble-induced turbulence, the profiles of the gas velocity are still only marginally impacted by the increased turbulence dispersion force.

The visualisation experiment demonstrates that the two-phase gas-liquid swirling flow quickly degrades and changes to a straight flow downstream of the swirler. With rising gas velocities or falling liquid velocities, the swirl decays quickly. A dispersion of the phases with values of ranging between 0 and 1 is noticed while examining the behaviour of the gas volume fraction over time (Fig. 14). This is related to a phenomena known as high flow instability, which prevents the interfacial compression method from accurately delineating the liquid and gas phases in some areas. Little bubble concentrations and high levels of turbulence are concentrated in the lowest part of the cyclonic chamber, which has an impact on the diffusion of the interface. Also, it is easy to see that over time, the liquid phase in this area gradually fills the chamber's volume.

Due to the difference in the densities of the phases subject to centrifugal forces, the liquid in the cyclonic chamber flows close to the walls while the gas is driven towards the inner core. It has been noted that the cyclonic chamber's inlet, where the centrifugal action is initiated, has the highest velocity. Its magnitude continuously lowers as the liquid moves higher towards the outflow along the cyclonic chamber. Because of the resistance produced by the

wall shear stress and the gravity field working opposite to the flow movement, decelerating the tangential component, this decrease in velocity illustrates that in a region sufficiently enough from the inlet, the flow would be totally axial. The swirl flow continues in the upward flow condition above the middle section of pipe. The size of the scattered bubbles at the swirling inlet plainly reduces as the liquid flow rate rises, but the centripetal force acting on these bubbles rises and takes over. The static pressure variation is shown in Fig. 15 at three locations where the pressure variation is significant near the inlet, while the constant pressure is maintained at the exit. The majority of the bubbles in the liquid slug at the entrance are then compelled to gather towards the pipe's axis, creating the so-called whirling gas trains. When the flow increases, the gas trains gradually spread out due to swirl decay and start to occupy the whole pipe channel in the downstream area. The dynamic pressure variation (Fig. 16) is more significant when compared to static pressure as the velocity variation due to swirl and differences in angular velocities of two phase flows. The dispersed bubbles in the swirling trains constantly collide and combine to eventually create a continuous gas column as the liquid flow rate rises over time. The distributed bubbles in the incoming liquid slug are fully separated once the whirling gas column is attained. This results in a very thick liquid layer and a very smooth gas-liquid interface between the gas column and the inner pipe wall.

The majority of the liquid phase flows as a thin liquid layer on the pipe wall when the inflow flow is annular flow, while the gas phase flows as a gas core in the pipe centre. The wall surface becomes partially wetted and the liquid phase flows if the liquid flow rate falls below a critical threshold. The tangential velocity of the gas and liquid flow decreases with swirl decay along the flow, increasing the screw pitch of the swirling ribbon. At the end, the rivulet flow returns after the ribbon flow has been twirling. The tangential injector-induced swirling gas-liquid flow exhibits the same swirling ribbon flow. A gas core formed in the middle as a result of centrifugal forces pushing the liquid phase against the pipeline wall. Three components of vorticities and their time variation near inlet, middle and exit portions of ascending pipe are plotted in Fig. 17. A revolving flow pattern replaced the intermittent gas-liquid flow pattern, and the scattered bubbles congregated into a gas vortex. It is possible to identify extremely intricate three-dimensional vortical flow structures connected to the phase transition. These vortical patterns are predominant near the pipe flow for both the phases (air and water), indicating the significance of the turbulent two-phase flow. In terms of the vortex shape, a significant portion of the vortical structures are visible at each timestep, close to the wall surface. Vortices that are close to the wall contribute more to the shearing effect than those that are farther away. The centre part of the pipe exhibits reduced vortex shedding and lower contact with the wall surface.

It is more difficult to find and identify a vortex in a flowfield. Coherent vortical features in the flow can be visualised to help with the flowfield's understanding. The Q-criterion factor, which consists of the symmetric part (strain rate tensor) and the antisymmetric part, can better demonstrate vortex visualisation (vorticity tensor). Variation of Q-criterion along the pipe-axis is plotted in Fig. 18. Range of Q-criterion varies from -300,000 (higher strain rate than vorticity) to 11,00,000 (Significant vortex than strain rate). A significant peak is observed at Z/L = 0.6, above the middle portion of the pipe. Visualization of Q-criterion (Fig. 19) enables to identify the combined gas-liquid flow under shear and strain for better output according to the phase. The straining rate increases near the walls while the vorticity magnitude is also observed to be higher at time = 0.25 s, 0.5 s, 0.75 s and 1 s. The shearing rate increases in the downstream along the core flow region with rotational rates (1/s) ranging from 0 to +1000. A gas core formed in the middle as a result of centrifugal forces pushing the liquid phase against the pipeline wall. A revolving flow pattern replaced the intermittent gas-

liquid flow pattern, and the scattered bubbles congregated into a gas vortex. The input's intermittent behaviour was maintained in both the gas and liquid phases. The primary distinction was how the bubbles in the liquid slug dispersed rather than how they accumulated in the middle of the pipeline due to centrifugal force. The distribution of the void fraction at the outputs similarly exhibited the slug flow pattern. The synchronised comparison demonstrated that the intermittent behaviour spread from the input to the outlets in addition to the symmetry in flow distribution.

Due to the conservation of angular momentum, vortex stretching is the lengthening of vortices in three-dimensional fluid flow, which is accompanied by an increase in the component of vorticity in the stretching direction. The process by which turbulence energy cascades from big to tiny scales is fundamentally described by vortex stretching (Fig. 20). Fluid elements are typically stretched out rather than compressed in turbulence. The mean vorticity across a vortex tube's cross-section should rise proportionately if its cross-section were to decrease. Volume conservation for incompressible flows implies that a tube's longitudinal stretching is proportionate to its transverse shrinking, which gives rise to the vortex stretching mechanism. The event proceeds in a time interval (0.5 s) and then vortex stretching term starts again. The inter-twining of both the stretching and squeezing processes is observed in a helical strand from inlet towards the exit. The gas phase created a symmetrical flow in the pipe at its centre, with an ascending liquid coating visible in the results. The gas vortex formed as a result of dispersed bubbles coming together due to centrifugal force within the cyclonic chamber. This behaviour aided the gas-liquid separation process by allowing smaller bubbles to be separated from the liquid bulk.

Fig. 21 shows the temporal variation of velocity components and volume fraction at the outlet. This indicates the yield and the behaviour of phase variation during the flow. Higher velocity components exist in the convergent geometry pipe, to maintain the continuity and outlet pressure as prescribed in other case also. The liquid fraction (α =1) is fast as compared in a convergent rather than a straight pipe flow due to the hydrodynamic boundary layer. Film flow is established to produce the better yield over a period of time for the constant boundary conditions maintained in the study.

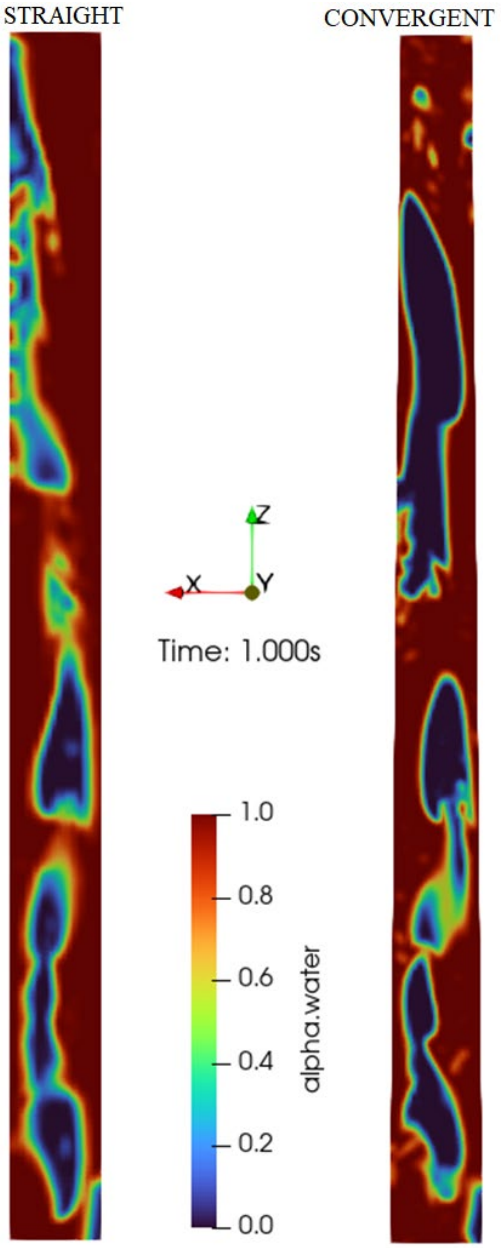

Fig. 5 Comparison of volume fraction contours in a bubble-slug transition flow at t = 1 s

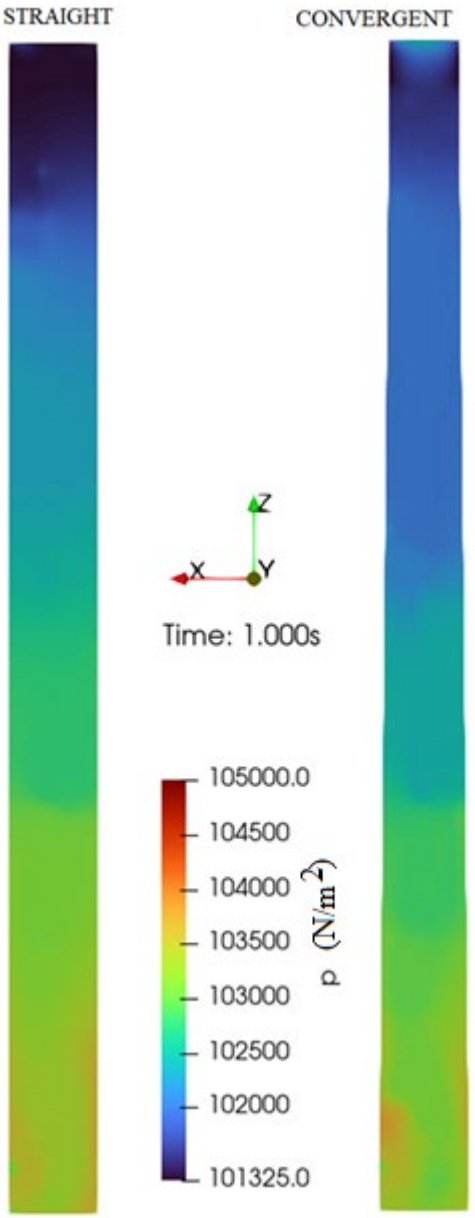

Fig. 6 Comparison of static pressure contours in a bubble-slug transition flow at t = 1 s

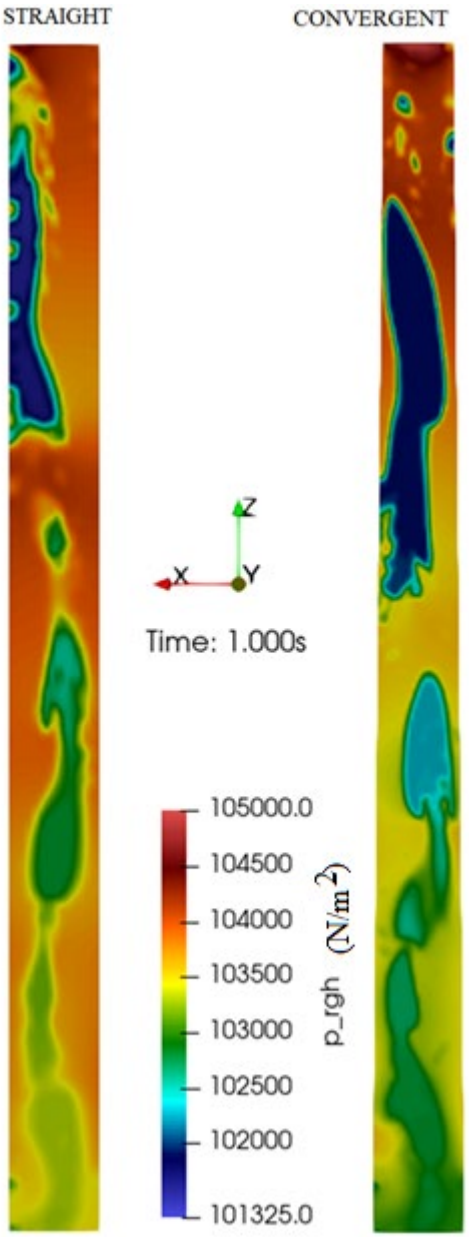

Fig. 7 Comparison of hydrodynamic pressure contours in a bubble-slug transition flow at t = 1 s

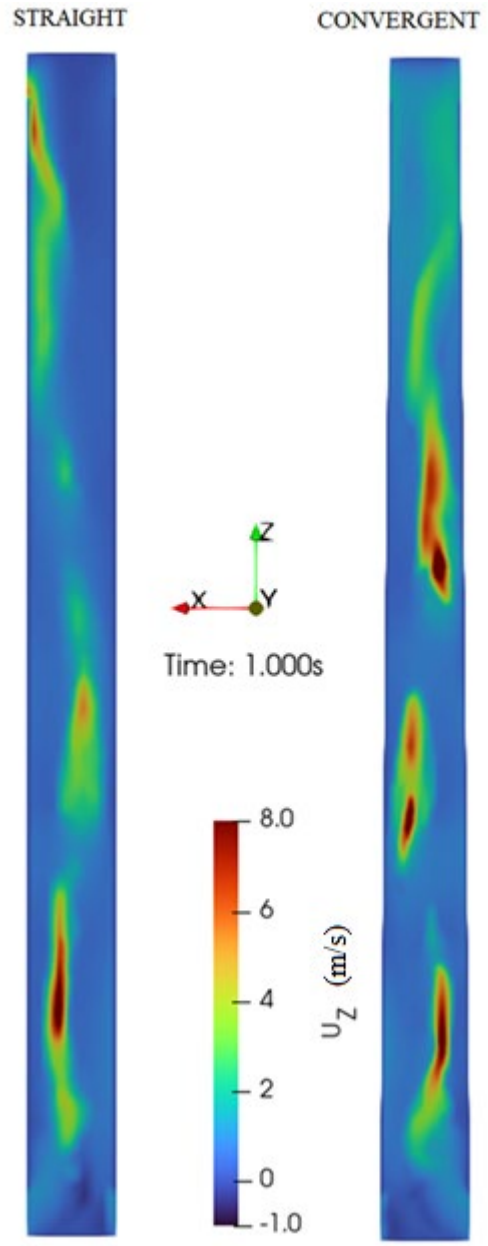

Fig. 8 Comparison of longitudinal velocity contours in a bubble-slug transition flow at t = 1 s

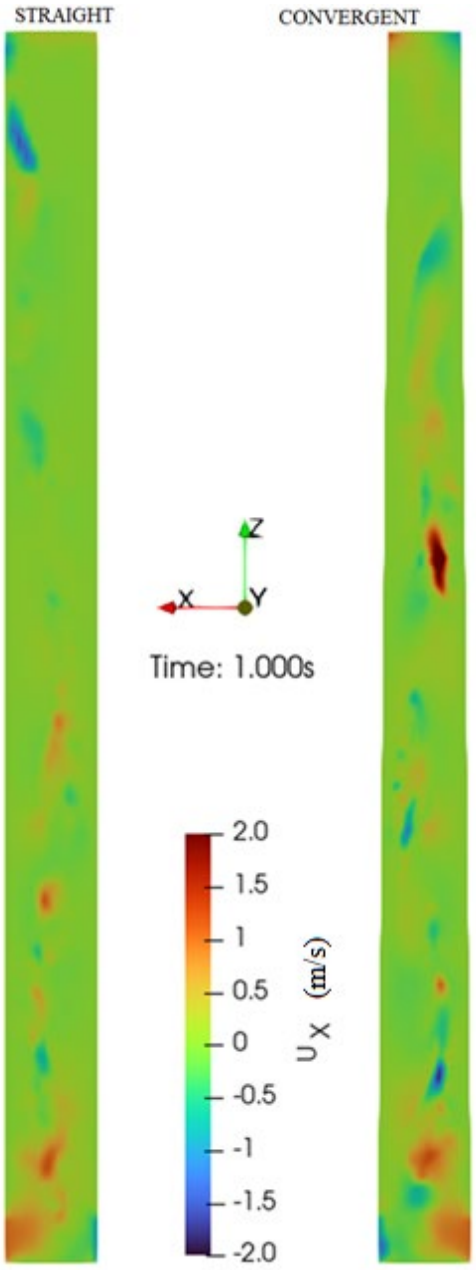

Fig. 9 Comparison of transverse velocity (along X) contours in a bubble-slug transition flow at t = 1 s

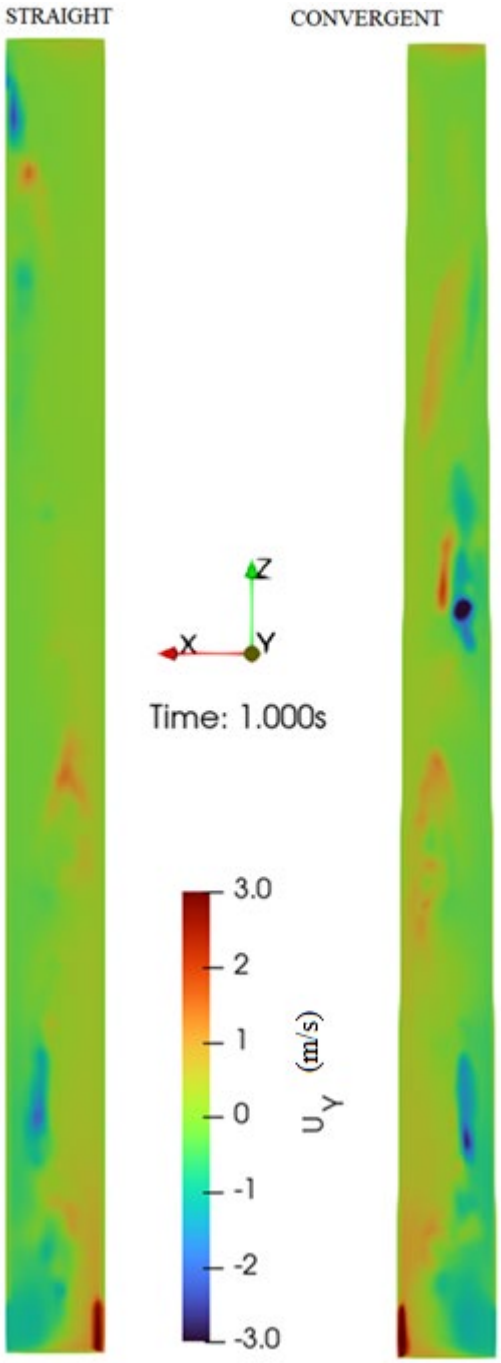

Fig. 10 Comparison of transverse velocity (along Y) contours in a bubble-slug transition flow at t = 1 s

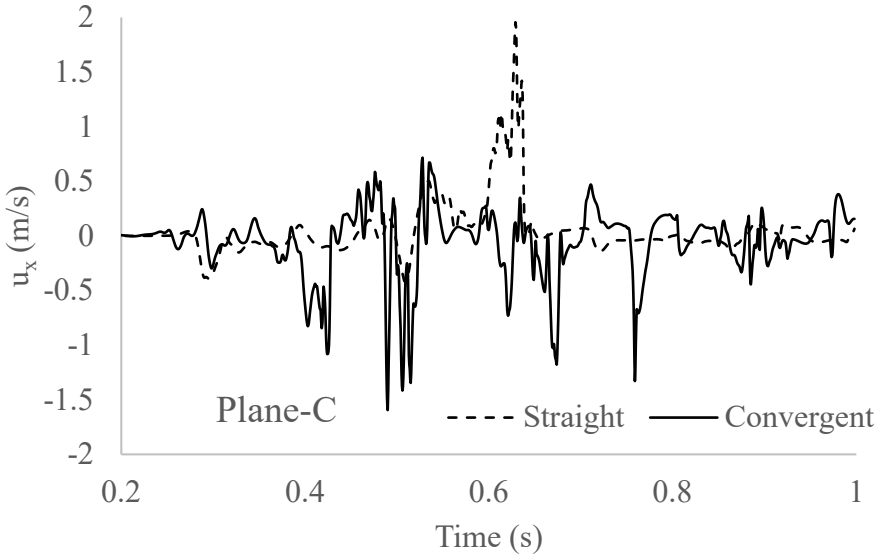

(a)

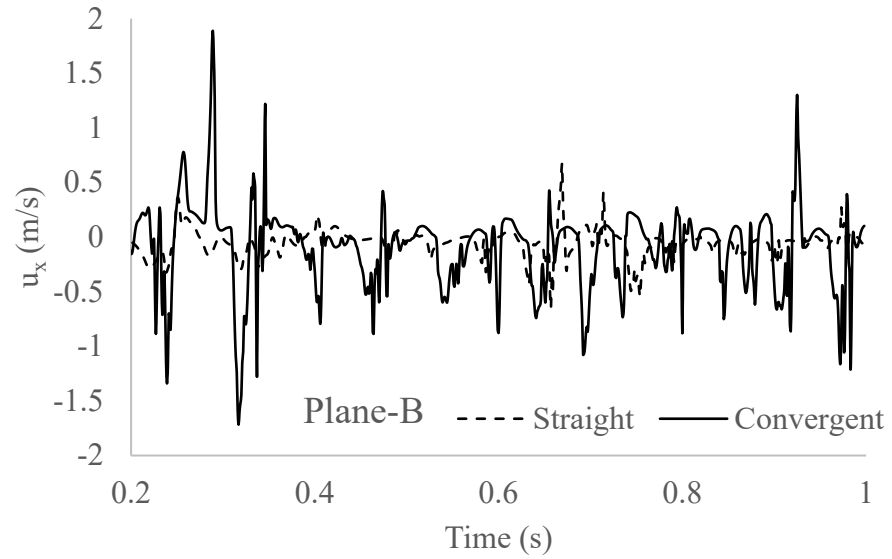

(b)

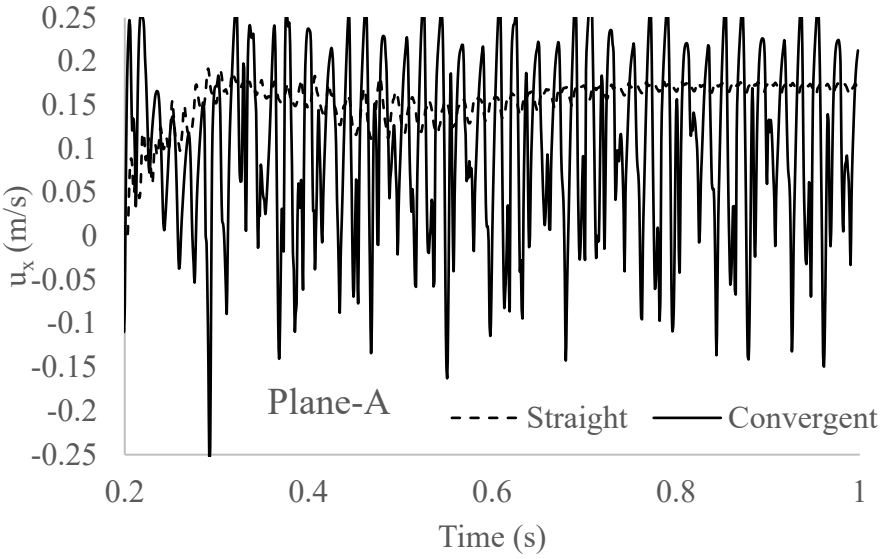

(c)

Fig.11 Illustration of transverse velocity (u_x) at respective planes (a) near pipe outlet (b) at centre of pipe (c) near pipe inlet

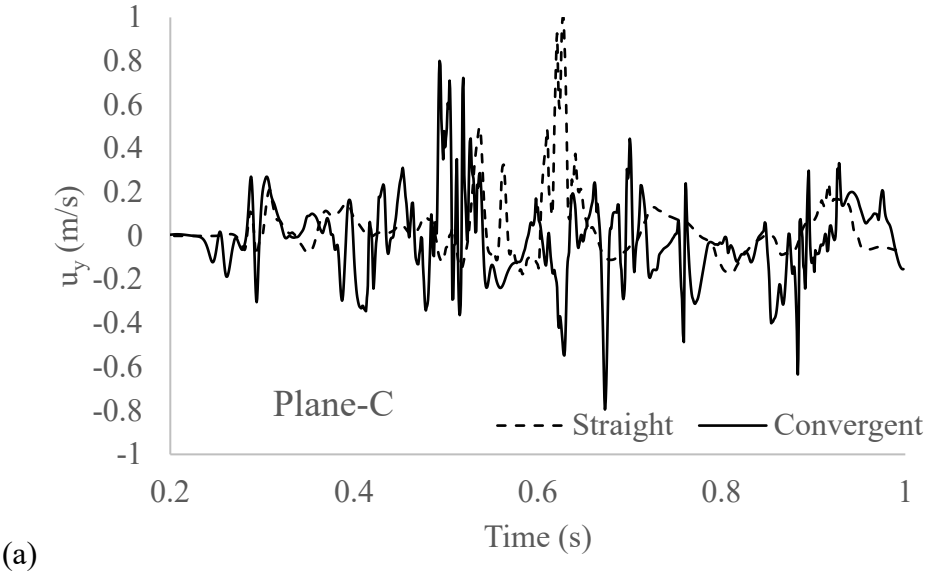

(a)

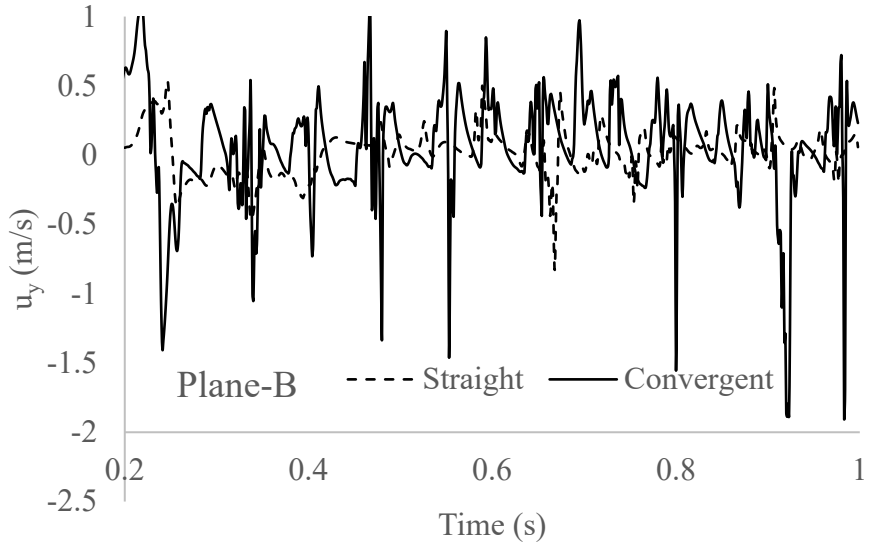

(b)

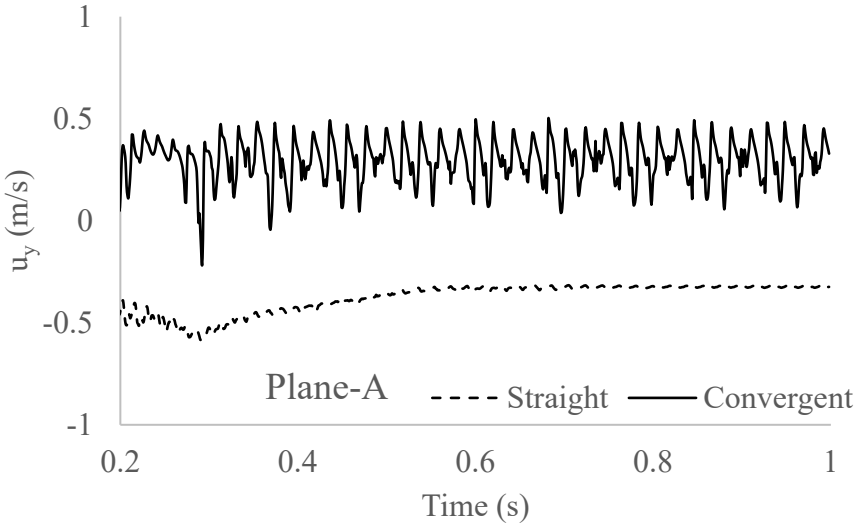

(c)

Fig.12 Illustration of transverse velocity (u_y) at respective planes (a) near pipe outlet (b) at centre of pipe (c) near pipe inlet

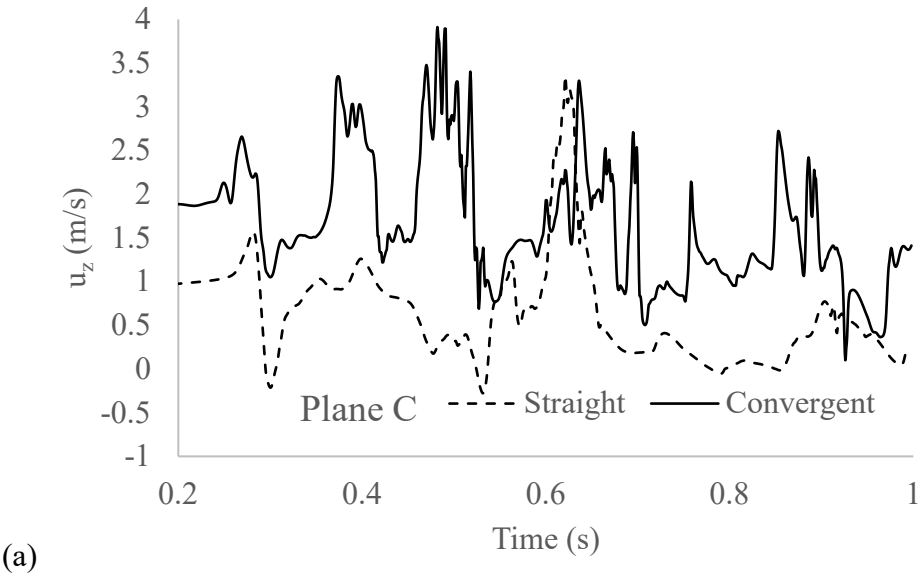

(a)

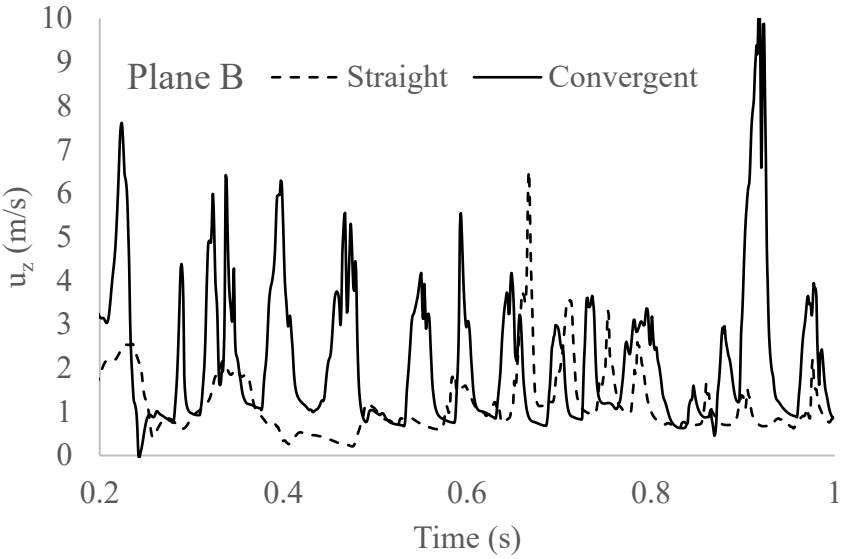

(b)

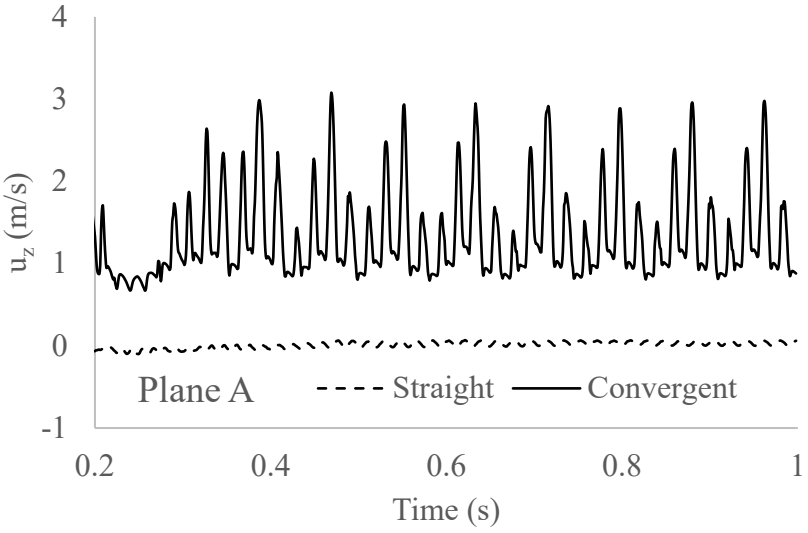

(c)

Fig.13 Illustration of longitudinal velocity (u_z) at respective planes (a) near pipe outlet (b) at centre of pipe (c) near pipe inlet

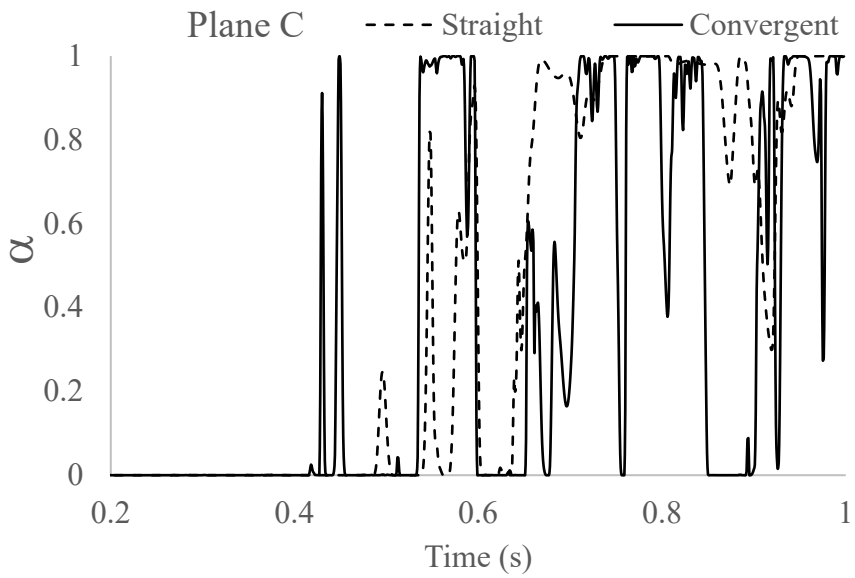

(a)

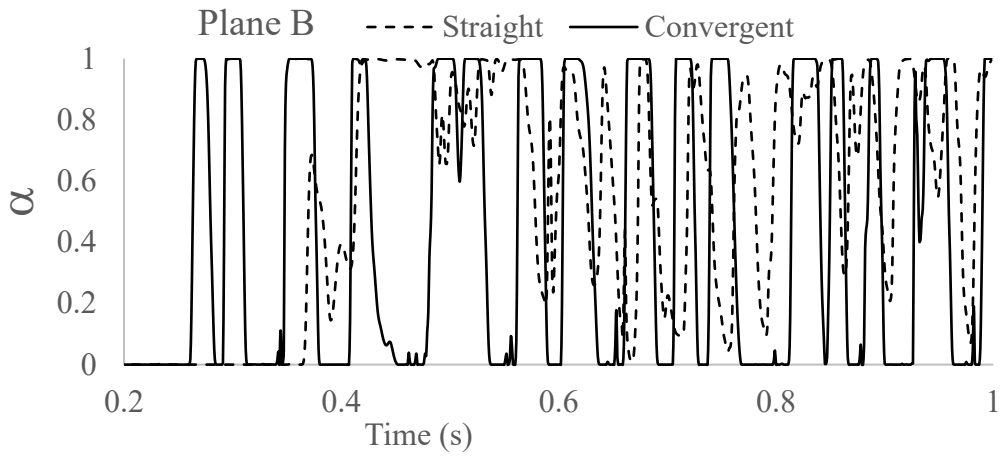

(b)

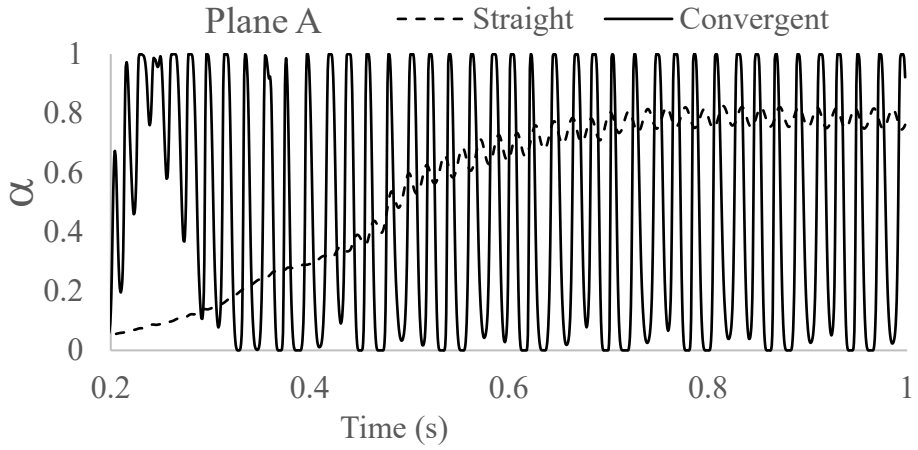

(c)

Fig.14 Illustration of volume fraction at respective planes (a) near pipe outlet (b) at centre of pipe (c) near pipe inlet

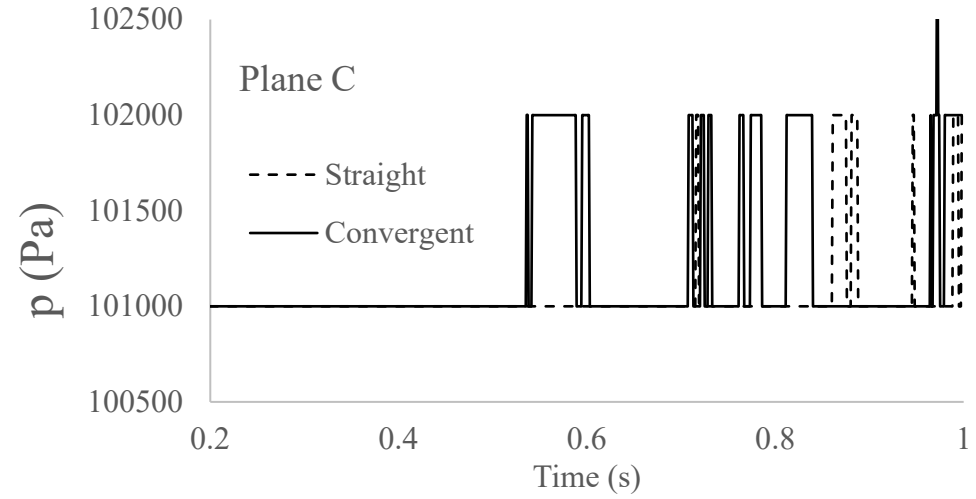

(a)

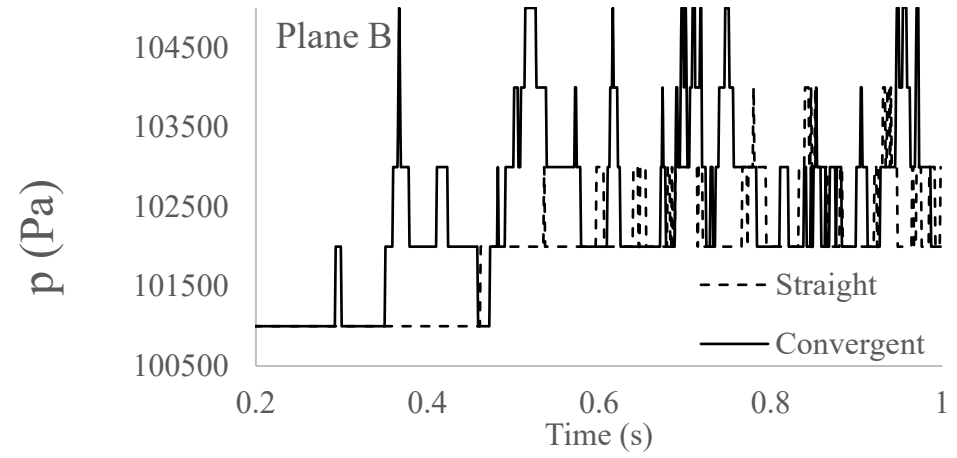

(b)

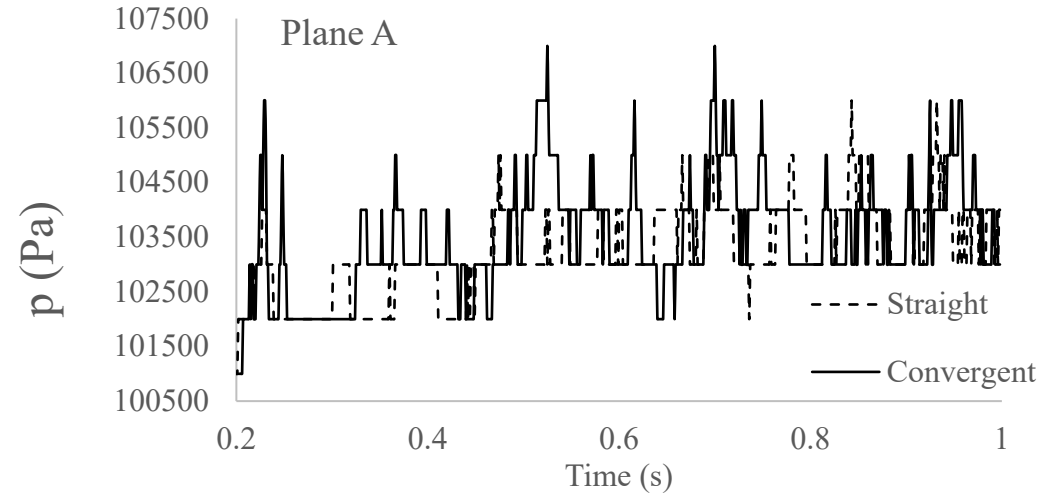

(c)

Fig.15 Illustration of Static pressure at respective planes (a) near pipe outlet (b) at centre of pipe (c) near pipe inlet

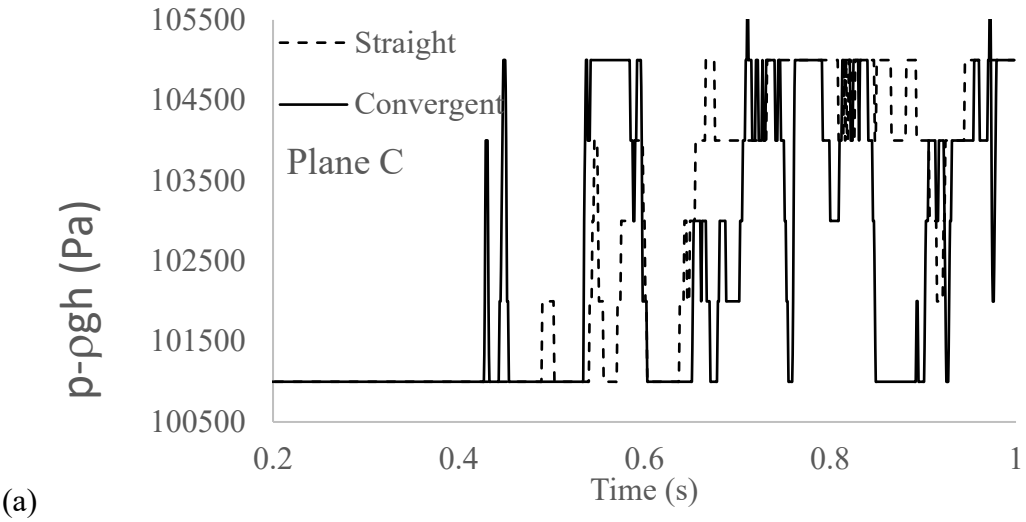

(a)

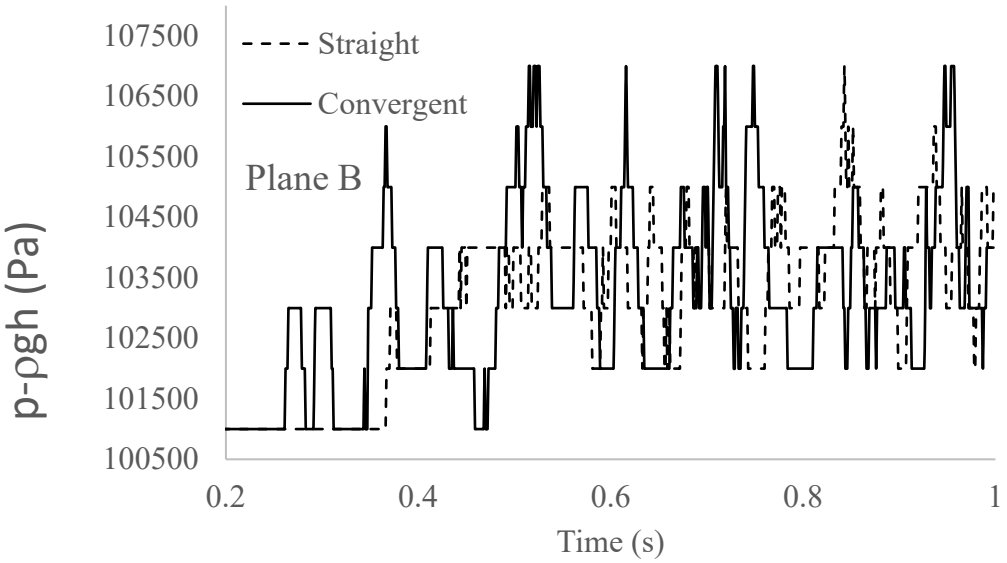

(b)

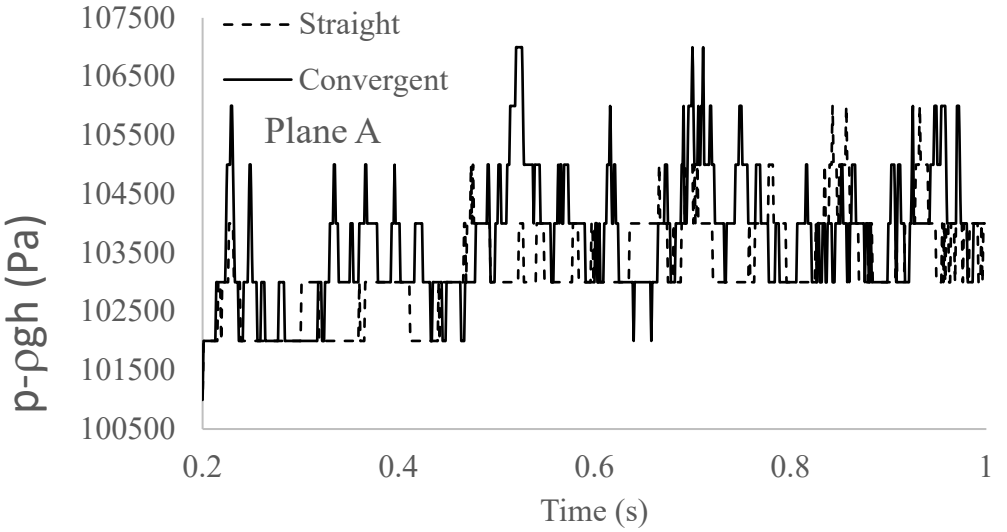

(c)

Fig.16 Illustration of hydrodynamic pressure at respective planes (a) near pipe outlet (b) at centre of pipe (c) near pipe inlet

(a)

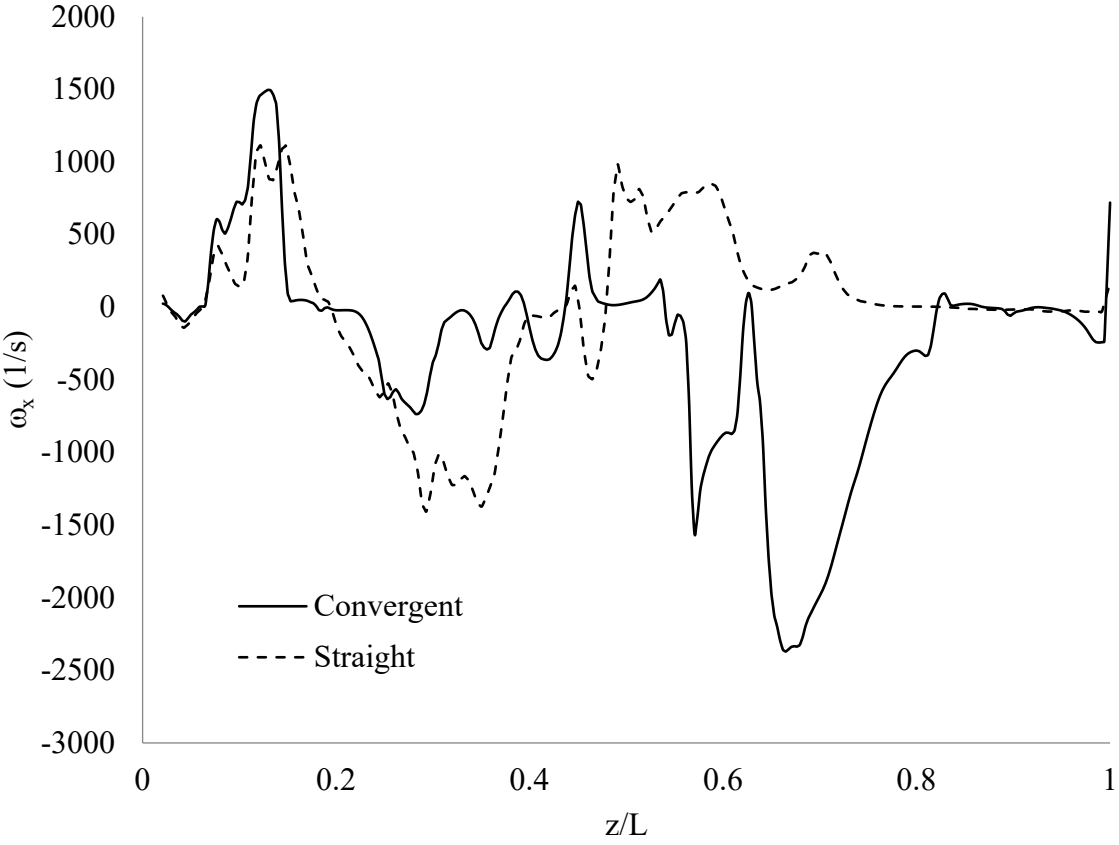
2000
1500
1000
500
0
-500
-1000
-1500
-2000
-2500
-3000
ωx (1/s)
Convergent
Straight
0
0.2
0.4
0.6
0.8
1
z/L

(b)

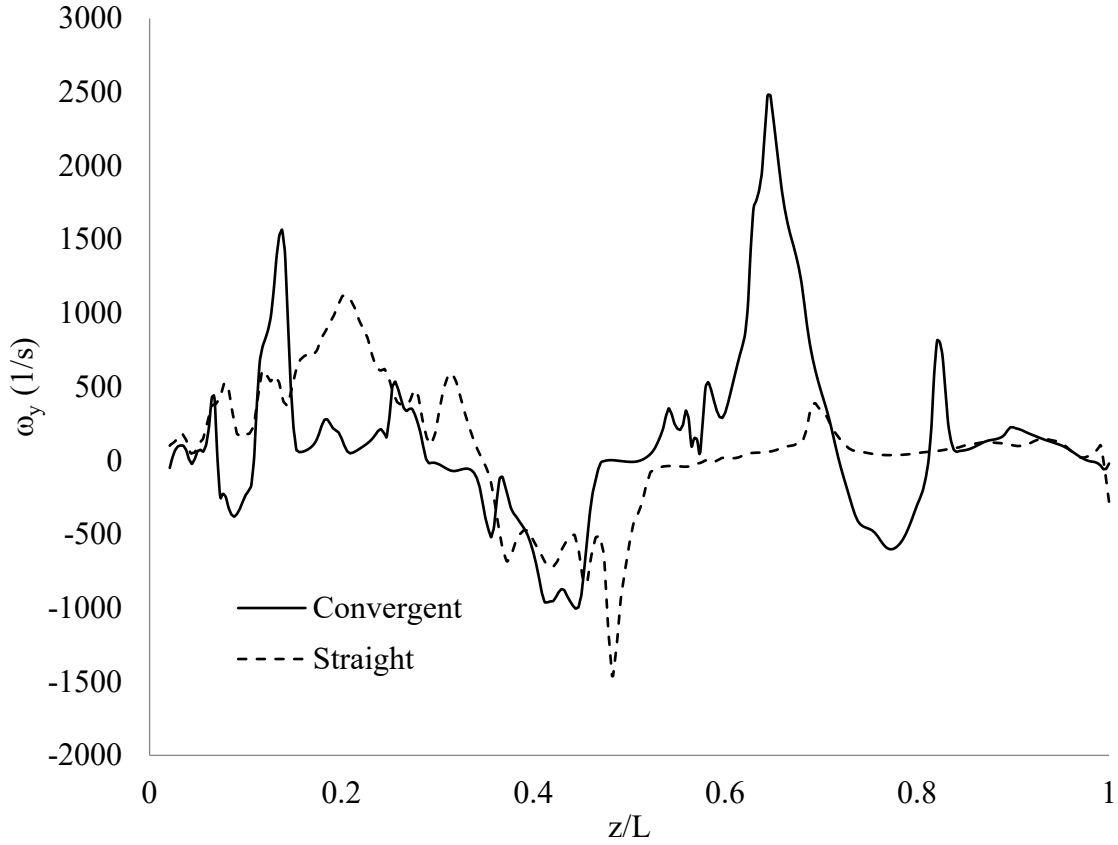
3000
2500
2000
1500
1000
500
0
-500
-1000
-1500
-2000
ωy (1/s)
Convergent
Straight
0
0.2
0.4
0.6
0.8
1
z/L

(c)

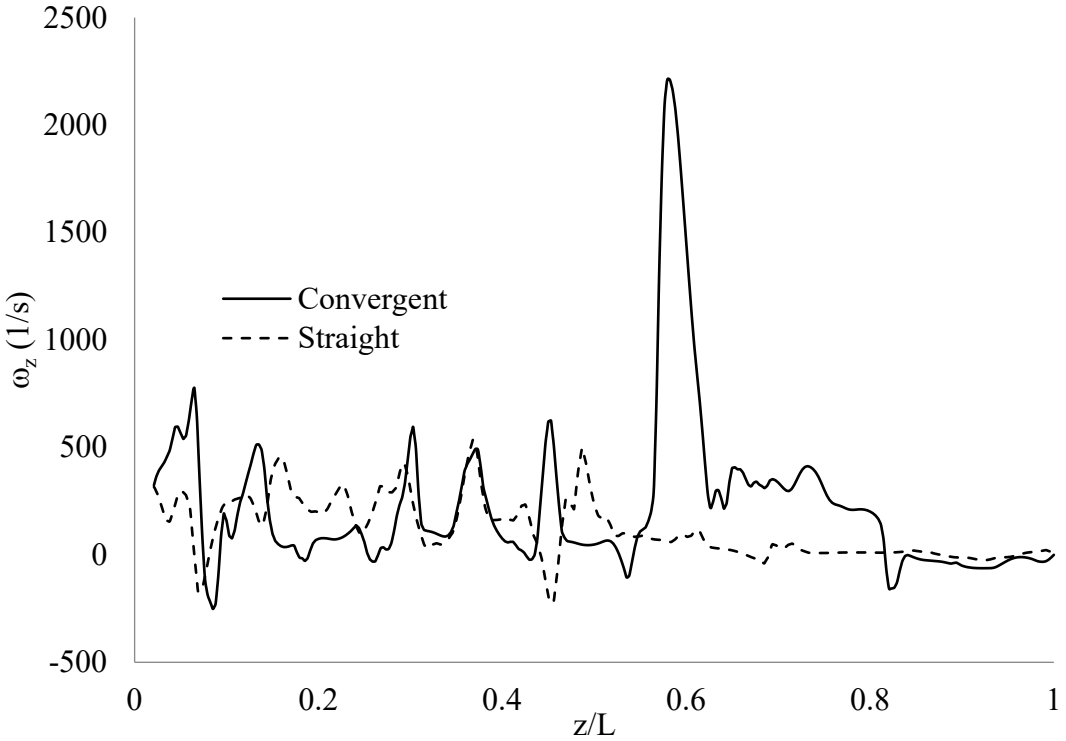

Fig.17 Variation of Vorticity components along the centre-line of the pipe at t=1 s (a) Transverse-x vorticity component (b) Transverse-y vorticity component (c) Longitudinal-z vorticity

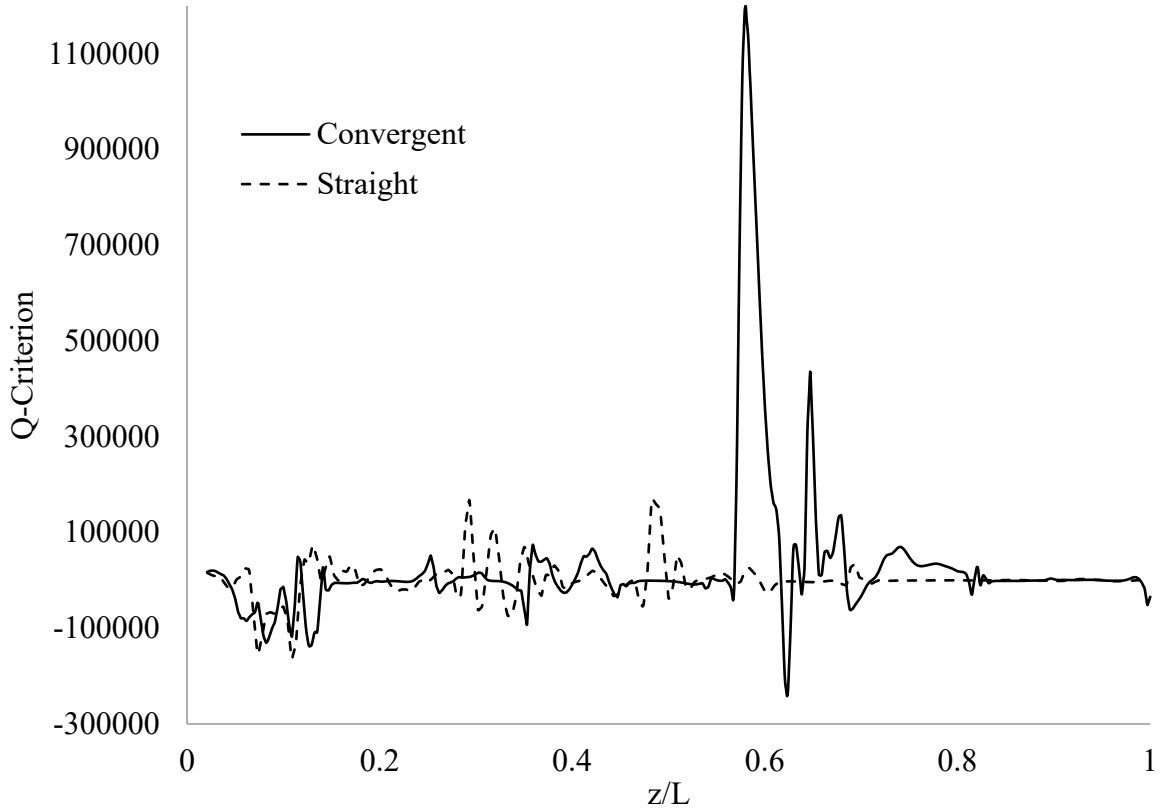

Fig.18 Variation of Q-criterion components along the centre-line of the pipe at t=1 s

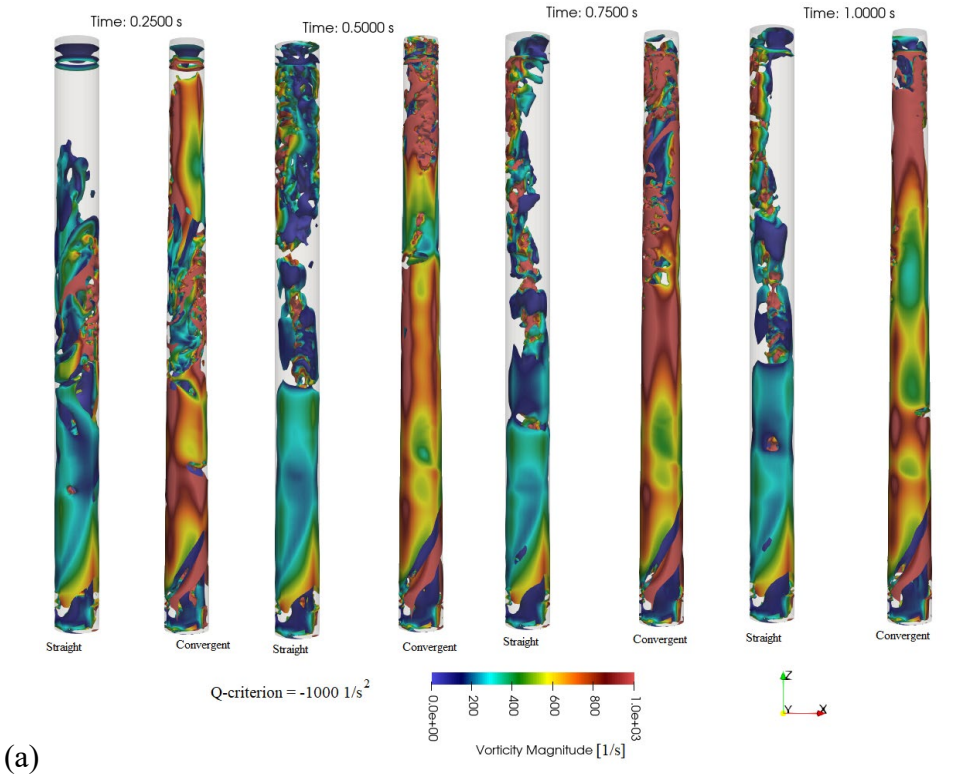

(a)

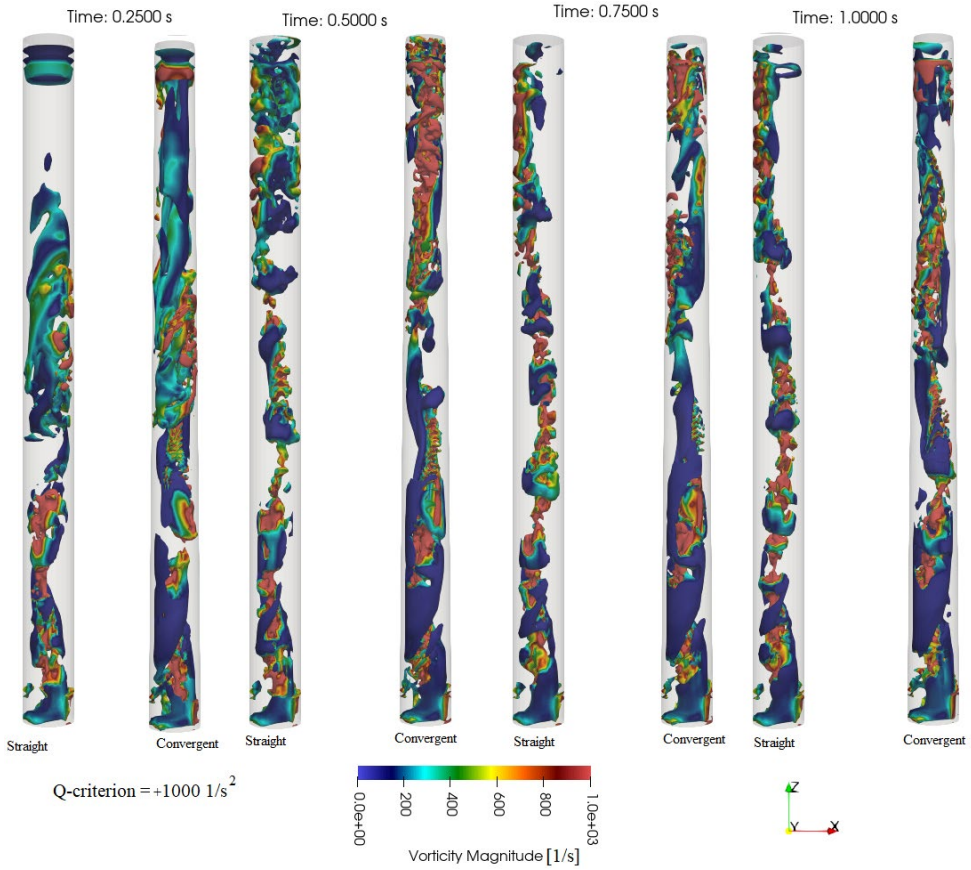

(b)

Fig.19 Time-series comparison of Q-criterion components coloured by vorticity magnitude (a) Q-criterion = -1000 $1/s^2$ (b) Q-criterion = + 1000 $1/s^2$

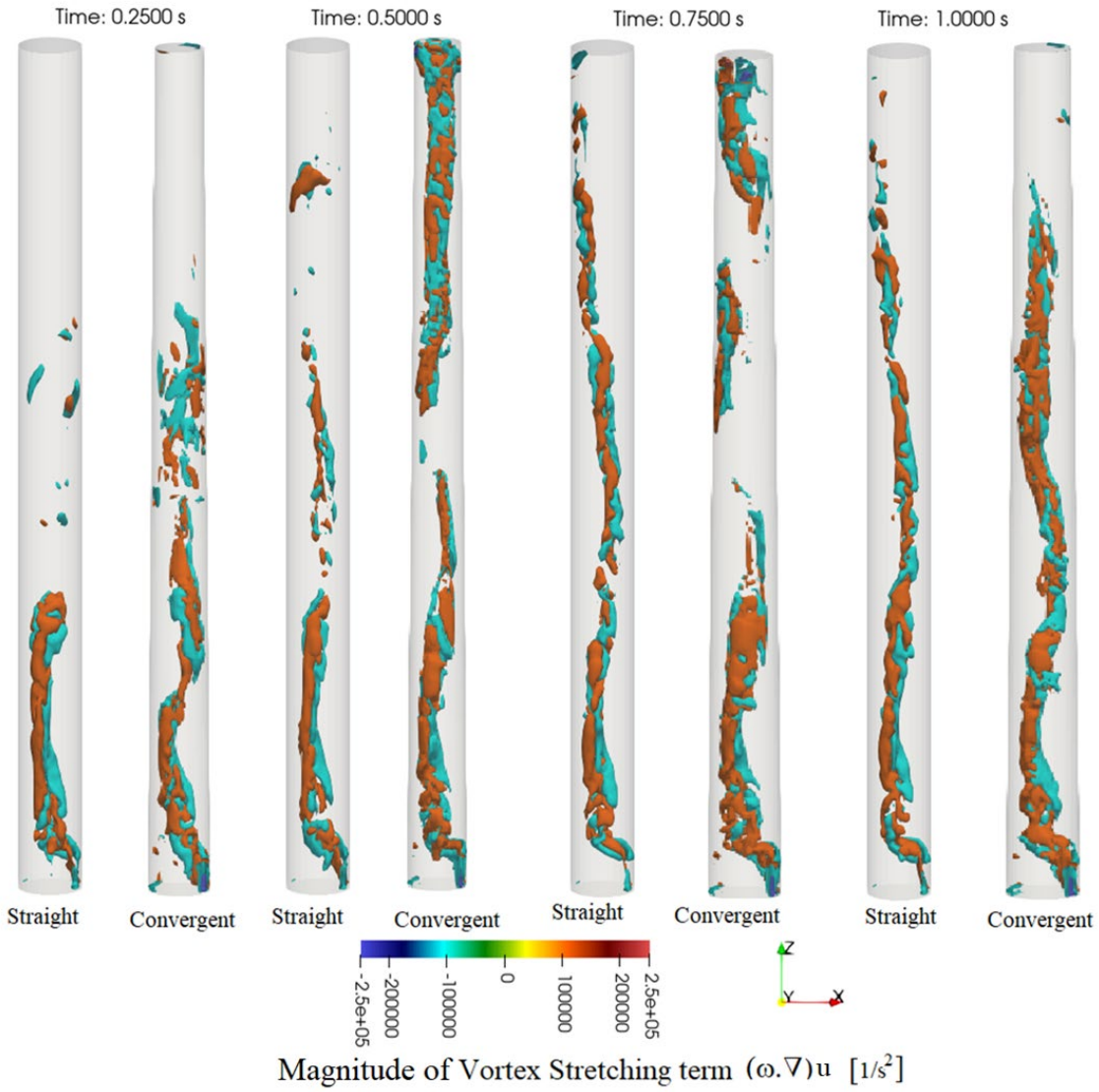

Fig.20 Time-series contours of vortex stretching term magnitude

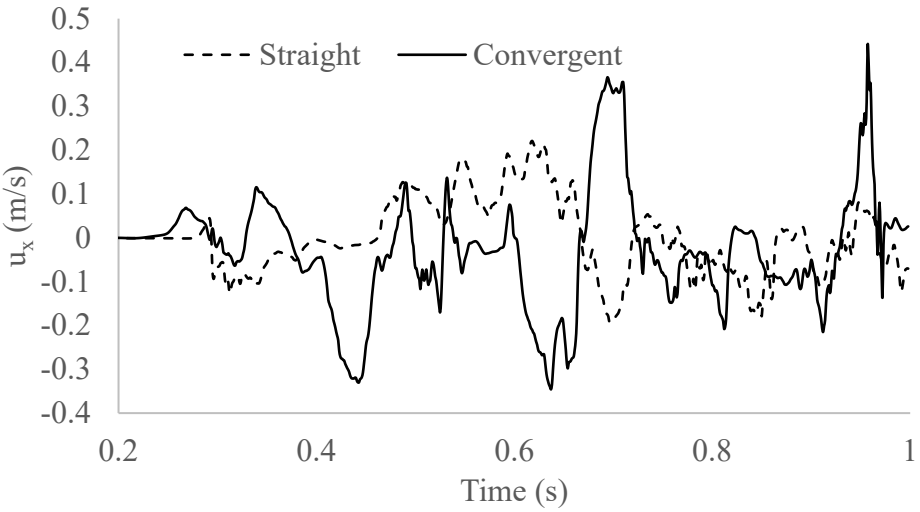

(a)

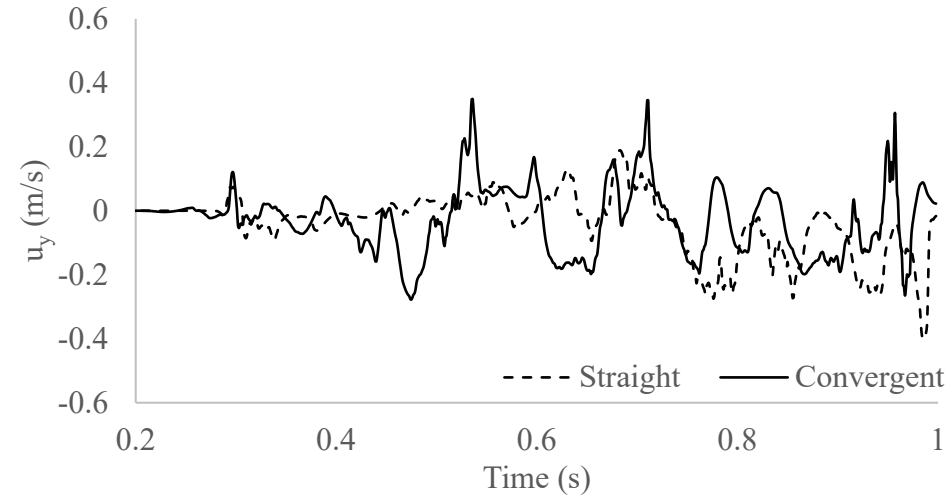

(b)

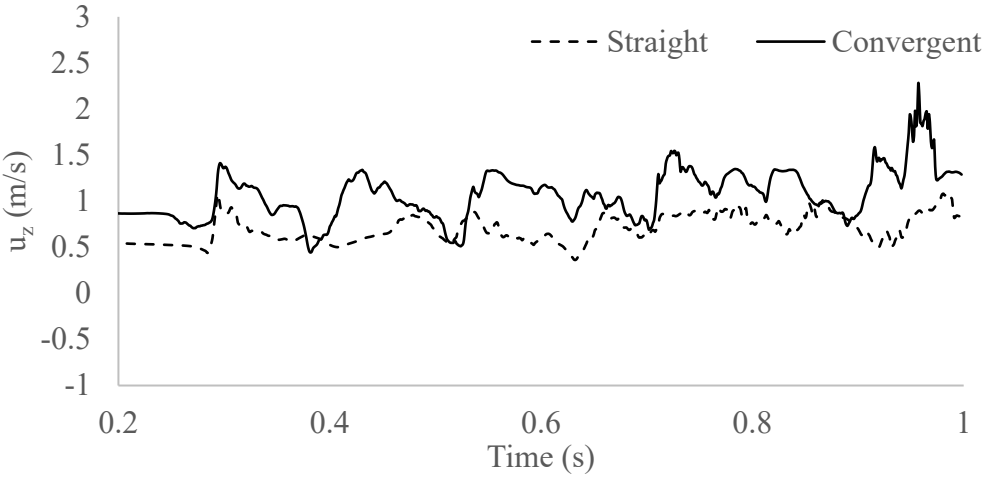

(c)

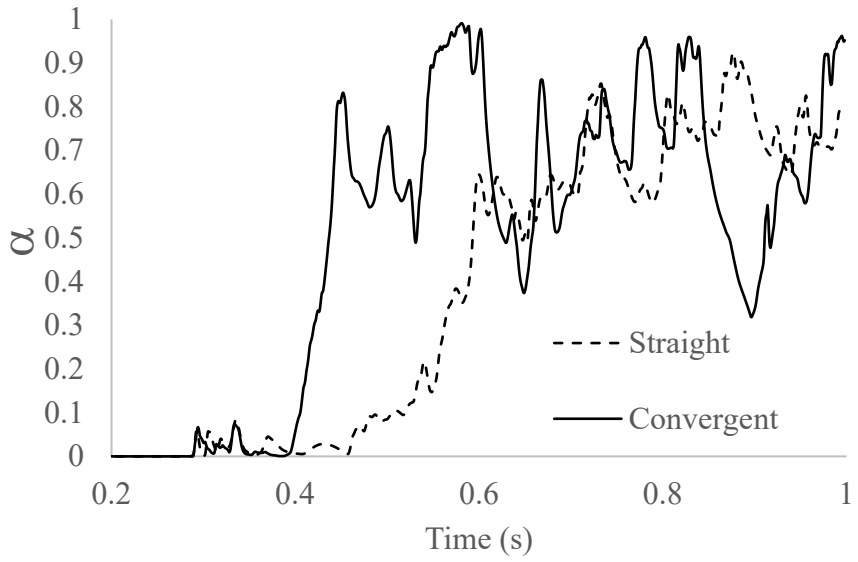

(d)

Fig.21 Time-series data of area averaged flow parameters at outlet (a) Transverse-x velocity (b) Transverse-y velocity (c) Longitudinal-z velocity (d) Volume fraction

Conclusion

Two phase flow investigations have been carried out in straight and convergent pipe of same diameter and same length using openFOAM in this numerical study. The inlet flow involves the tangential components of velocity with air and water phase and the outlet is maintained with the specified pressure. Validation of two phase flow is carried out with the experimental (wire mesh sensor) data and the numerical study of Eidt et al. (2021). The errors between the present numerical output and experimental literature results are accounted, but found within the suitable agreement. These errors arise due to the limited model capability in predicting the fluid characteristics and flow physics. The first order models are employed in gradient and divergence terms in the equations described earlier, while Van Leer model is accounted for evaluating the volume fraction. Second order upwind schemes could be employed in order to reduce the error gap arisen between experiments and CFD. Further the study involved the comparison of flow parameters such as velocity components, hydrodynamic pressure, volume fraction between straight and convergent pipes. In order to understand the rotational flow, vorticity components, Q-criterion and vortex stretching terms are studied in detail. The following results are found from the present study.

- Normalized film thickness (δ/R) is found to vary between 0.4 and 0.6, which closely agrees with wire-mesh sensor (WMS) data by Eidt et al. (2021).
- The variation in hydrodynamic pressure affects the slug and bubble flow region, found to be apparent in the top portion of the pipe.
- Transverse velocity component variations are lower as compared to longitudinal velocity at all the three inspection planes.
- Longitudinal velocity appears to be higher at the core in both the straight and convergent cases due to the no-slip wall condition near the walls.
- Q-criterion is found to be significantly higher in convergent pipe at 60 % of its length from inlet.
- From the understanding on the vortex-stretching term, the inter-twining of both the stretching and squeezing flow processes is observed in a helical strand from inlet towards the exit.

The above listed factors promote the increase in the output liquid yield of convergent pipe outlet by 17 %. The convergent pipe makes the flow to transition from bubble flow to slug flow. From the numerical results obtained in this study, the hypothesis is successfully verified to prove the higher percentage of liquid (oil) extraction in convergent pipe as compared to a constant area pipe.

Data Availability Statement

All the data in this study are obtained using OpenFOAM software. The data will be made available via correspondence as per the request by an email.

Declaration of competing interest

The author declares there is no known competing financial interests or personal relationships that could have appeared to influence the work reported in this study.

Nomenclature

i	intensity
j	superficial velocity
k	turbulence kinetic energy
l	characteristic length
p	pressure
r	radius of pipe

t time
u velocity

Subscripts
g gaseous phase (air)
l liquid phase (water)
ref reference
x component, coordinate axis
y component, coordinate axis
z component, coordinate axis

Symbols
α volume fraction
∇ gradient operator
δ average liquid film thickness
ρ density of fluid
σ surface tension coefficient
ω vorticity, turbulence specific dissipation rate

References

1. Adaze, E., Badr, H.M., and Al-Sarkhi, A., CFD modeling of two-phase annular flow toward the onset of liquid film reversal in a vertical pipe, *Journal of Petroleum Science and Engineering,* vol. 175, pp. 755-774, 2019.
2. Adineh, M., Nematollahi, M., and Erfaninia, A., Experimental and numerical void fraction measurement for modeled two-phase flow inside a vertical pipe, *Annals of Nuclear Energy,* vol. 83, pp. 188-192, 2015.
3. Ameri, M., and Tirandaz, N., Two phase flow in a wavy core-annular configuration through a vertical pipe: Analytical model for pressure drop in upward flow, *International Journal of Mechanical Sciences,* vol. 126, pp. 151-160, 2017.
4. Atmani, H., Zamansky, R., Climent, E., and Legendre, D., Stochastic wall model for turbulent pipe flow using Immersed Boundary Method and Large Eddy Simulation, *Computers & Fluids,* vol. 239, p. 105419, 2022.
5. Cailly, W., Walaszek, H., Brzuchacz, S., Zhang F., and Lasaygues, P., Pipe two-phase flow non-invasive imaging using Ultrasound Computed Tomography: A two-dimensional numerical and experimental performance assessment, *Flow Measurement and Instrumentation,* vol. 74, p. 101784, 2020.
6. Cao, X., Yang, K., Wang H., and Bian J., Gas–liquid–hydrate flow characteristics in vertical pipe considering bubble and particle coalescence and breakage, *Chemical Engineering Science,* vol. 252, p. 117249, 2022.
7. Carlos, P., Song, B., and Avila, M., Direct numerical simulation of two-phase pipe flow: Influence of the domain length on the flow regime, *International Journal of Multiphase Flow,* vol. 144, p. 103786, 2021.
8. Dong, C. and Hibiki, T., Correlation of heat transfer coefficient for two-component two-phase slug flow in a vertical pipe, *International Journal of Multiphase Flow,* vol. 108, pp. 124-139, 2018.

9. Dziubinski, M., Fidos, H., and Sosno, M., The flow pattern map of a two-phase non-Newtonian liquid–gas flow in the vertical pipe, *International Journal of Multiphase Flow,* vol. 30, pp. 551-563, 2004.
10. Eidt, J., Henrique, K., Carolina C. R., Rafael D., César Y.O, Dalton B., Marco J.D.S., Flávio N.J., Paulo H.D.S., and Rigoberto E.M.M., Numerical and experimental analysis of vertically ascending swirling liquid film flow, *Journal of Petroleum Science and Engineering*, vol. 206, p.109030, 2021.
11. Faghihi, R., Nematollahi, M., Erfaninia A., and Adineh, M., Void fraction measurement in modeled two-phase flow inside a vertical pipe by using polyethylene phantoms, *International Journal of Hydrogen Energy,* vol. 40, pp. 15206-15212, 2015.
12. Issa, S.A., and Lucas, D., Two phase flow 1D turbulence model for poly-disperse upward flow in a vertical pipe, *Nuclear Engineering and Design,* vol. 239, pp. 1933-1943, 2009.
13. Long, J., Yang, B.W., Zhang, B., and Wang, S., Computational case study on upward two-phase flow in vertical circular pipe based on CFD approach: Multidimensional flow instabilities investigation, *Progress in Nuclear Energy,* vol. 144, p. 104085, 2022.
14. Lucas, D., Beyer, M., Kussin J., and Schütz, P., Benchmark database on the evolution of two-phase flows in a vertical pipe, *Nuclear Engineering and Design,* vol. 240, pp. 2338-2346, 2010.
15. Martin N.K, Bieberle, A. and Hampel, U., Investigations on bubbly two-phase flow in a constricted vertical pipe, *International Journal of Multiphase Flow,* vol. 130, p. 103340, 2020.
16. Ohnuki, A. and Akimoto, H., Experimental study on transition of flow pattern and phase distribution in upward air–water two-phase flow along a large vertical pipe, *International Journal of Multiphase Flow,* vol. 26, pp. 367-386, 2000.
17. Pouryoussefi, S. M., and Zhang, Y., Identification of two-phase water–air flow patterns in a vertical pipe using fuzzy logic and genetic algorithm, *Applied Thermal Engineering,* vol. 85, pp. 195-206, 2015.
18. Prasser, H.M., Beyer, M., Carl, H., Gregor, S., Lucas, D., Pietruske, H., Schütz, P., and Weiss, F.P., Evolution of the structure of a gas–liquid two-phase flow in a large vertical pipe, *Nuclear Engineering and Design,* vol. 237, pp. 1848-1861, 2007.
19. Rajab, O., Hewakandamby, B., Azzi A., and Azzopardi, B., Fluid structure behaviour in gas-oil two-phase flow in a moderately large diameter vertical pipe, *Chemical Engineering Science,* vol. 187, pp. 377-390, 2018.
20. Rinne, A. and Loth, R., Development of local two-phase flow parameters for vertical bubbly flow in a pipe with sudden expansion, *Experimental Thermal and Fluid Science,* vol. 13, pp. 152-166, 1996.
21. Saidj, F., Hasan, A., Bouyahiaoui, H., Zeghloul, A., and Azzi, A., Experimental study of the characteristics of an upward two-phase slug flow in a vertical pipe, *Progress in Nuclear Energy,* vol. 108, pp. 428-437, 2018.
22. Sibel T.K., Martin N.K., Yixiang L., Eckhard K., Uwe H., CFD simulation of bubbly flow around an obstacle in a vertical pipe with a focus on breakup and coalescence modelling, *International Journal of Multiphase Flow*, vol.135, p.103528, 2021.

23. Shawkat, M. E., Ching, C. Y., and Shoukri, M., On the liquid turbulence energy spectra in two-phase bubbly flow in a large diameter vertical pipe, *International Journal of Multiphase Flow,* vol. 33, pp. 300-316, 2007.
24. Szalinski, L., Abdulkareem, L. A., Silva, M. J. D., Thiele, S., Beyer, M., Lucas, D., Perez, V. H., Hampel, U., and Azzopardi, B. J., Comparative study of gas–oil and gas–water two-phase flow in a vertical pipe, *Chemical Engineering Science,* vol. 65, pp. 3836-3848, 2010.
25. Tas-Koehler, S., Neumann-Kipping, M., Liao, Y., Krepper, E., and Hampel, U., CFD simulation of bubbly flow around an obstacle in a vertical pipe with a focus on breakup and coalescence modelling, *International Journal of Multiphase Flow,* vol. 135, p. 103528, 2021.
26. Zeguai, S., Chikh, S., and Tadrist, L., Experimental study of air-water two-phase flow pattern evolution in a mini tube: Influence of tube orientation with respect to gravity, *International Journal of Multiphase Flow,* vol. 132, p. 103413, 2020.